

**Target-cell-specific Left-Right Asymmetry of NMDA Receptor
Content in Schaffer Collateral Synapses in $\epsilon 1$ Knock-out Mice**

Yue Wu

DOCTOR OF PHILOSOPHY

Department of Physiological Science
School of Life Science
The Graduate University for Advanced Studies

2004

CONTENTS

Abstract	P. 3
Introduction	P. 6
Material and Methods	P. 10
Results	P. 22
Discussion	P. 34
Acknowledgement	P. 42
References	P. 43
Figures and Tables	P. 53

Abstract

N-methyl-D-aspartate (NMDA) receptors mediate excitatory neurotransmission and activity-dependent changes in synaptic efficacy in the central nervous system and play an important role in learning and memory. NMDA receptors are composed of seven known subunits- GluR ζ 1 (NR1), GluR ϵ 1-4 (NR2A-2D) and GluR χ 1-2 (NR3A-3B), and functional activities of the NMDA receptor channel require the heteromeric assemblies of obligatory GluR ζ 1 with one or more other subunits.

In the hippocampal CA1 area, pyramidal cells and GABAergic interneurons receive excitatory inputs from Schaffer collaterals (Sch) arising from the ipsilateral CA3 pyramidal neurons and commissural fibers (com) arising from the contralateral CA3 pyramidal neurons (Ishizuka et al., 1990). The fast excitatory synaptic transmission from these inputs is mostly mediated by NMDA and AMPA type glutamate receptors. The NMDA receptors in the Sch and com fiber synapses on pyramidal cells contain ζ 1, ϵ 1, and ϵ 2 subunits in adult rodents (Monyer et al., 1994; Fritschy et al., 1998; Takumi et al., 1999; Racca et al., 2000). Some interneurons in the hippocampus also express ϵ 4 subunit as well as ζ 1, ϵ 1, and ϵ 2 subunits (Monyer et al., 1994; Standaert et al., 1996; Standaert et al., 1999).

The asymmetrical allocation of NMDA receptor ϵ 2 (NR2B) subunits was discovered in the Sch-CA1 pyramidal cell synapses between the left and right hippocampus and between the apical and basal dendrites of single neurons (Kawakami et al., 2003). Direction of this asymmetry depends on inputs; com-pyramidal cell synapses have a mirror-image asymmetry to that for Sch-pyramidal cell synapses (Kawakami et al., 2003). Although electrophysiological and morphological studies have suggested differential localization of glutamate receptors depending on target-cell types as well as

on input pathways (Shigemoto et al., 1996; Nusser et al., 1998b; Gottmann et al., 1997; Ito et al., 2000), it is not clear whether the asymmetry in $\epsilon 2$ allocation is also related to the types of the postsynaptic cells. In the present study, to examine the asymmetrical $\epsilon 2$ distribution in distinct postsynaptic target cells, I utilized quantitative postembedding immunogold labeling method in the left and right CA1 areas. I used $\epsilon 1$ knock-out (KO) mice to facilitate the detection of difference in the $\epsilon 2$ immunoparticle density.

In naïve $\epsilon 1$ KO mice, I found no significant left-right difference in labeling density for $\epsilon 2$ in pyramidal cell synapses, which are made by both Schaffer collateral and commissural fibers. However, in $\epsilon 1$ KO mice operated for ventral hippocampal commissure transection (VHCT) to examine Schaffer collateral synapses selectively, labeling density for $\epsilon 2$ but not $\zeta 1$ and GluR2/3 in Sch-CA1 pyramidal cell synapses was significantly different ($P < 0.05$) between the left and right hippocampus. The ratio of $\epsilon 2$ labeling density in the left to right was about 1:1.5 in the stratum oriens and about 1.6: 1 in the stratum radiatum. Moreover, labeling density for $\epsilon 2$ in Sch-CA1 pyramidal cell synapses was significantly different ($P < 0.05$) between basal and apical dendrites. The ratio of $\epsilon 2$ labeling density in the basal to apical dendrites was about 1:1.4 in the left hippocampus and about 1.5:1 in the right hippocampus. This result is consistent with the asymmetry in $\epsilon 2$ allocation previously detected with electrophysiology and immunoblot analysis in wild type mice. On the other hand, the $\epsilon 2$ labeling density was not significantly different ($P > 0.05$) in interneuron synapses between the left and right. Interneurons were grouped into GluR4-immunopositive and GluR4-immunonegative subpopulations in the stratum radiatum. Double immunofluorescence results showed that 88.7% of GluR4-immunopositive interneurons were palvalbumin immunoreactive and 11.1% of GluR4-immunopositive interneurons were mGluR1 α immunoreactive.

None of GluR4-immunopositive interneurons showed immunoreactivity for calretinin or calbindin. The density ratio of $\epsilon 2$ labeling in the left to right was 0.88:1 in Sch-GluR4 immunopositive interneuron synapses and 1.14: 1 in Sch-GluR4 immunonegative interneuron synapses.

Consistent with the anatomical asymmetry in the $\epsilon 2$ distribution in Sch-CA1 pyramidal cell synapses, amplitude of evoked NMDA EPSCs relative to that of non-NMDA EPSCs was different between the left and right CA1 area in VHCT-operated $\epsilon 1$ KO mice. The amplitude ratio of AP5-sensitive EPSCs to DNQX-sensitive EPSCs was larger in the right than left stratum oriens (left, $21.6\% \pm 2.64$, $n = 5$ from 5 animals; right, $40.2\% \pm 3.40$, $n = 5$, from 5 animals; $P < 0.01$, t -test.). By contrast, the ratio in the stratum radiatum showed a mirror-image asymmetry to that found in the stratum oriens (left, $39.3\% \pm 3.40$, $n = 6$, from 6 animals; right, $16.4\% \pm 3.11$, $n = 5$, from 5 animals; $P < 0.01$, t -test). Moreover, the asymmetrical $\epsilon 2$ content was directly reflected in different amplitudes of long-term potentiation (LTP) in the left and right stratum radiatum in VHCT-operated $\epsilon 1$ KO mice: in the left Sch-CA1 synapses, the amplitude of LTP was higher than that in the right Sch-CA1 synapses (left, $138\% \pm 2.76$, $n = 7$, from 7 animals; right, $104\% \pm 2.77$, $n = 6$, from 6 animals, $P < 0.05$, t -test).

The study indicates that the target-cell-specific left-right asymmetry of $\epsilon 2$ distribution results in the left-right difference in NMDA receptor content in Sch-CA1 pyramidal cell synapses in $\epsilon 1$ KO mice.

Introduction:

Glutamate receptors (GluRs) mediate most of the excitatory neurotransmission, and plastic changes in excitatory synaptic transmission in the central nervous system (CNS). In addition, they are also involved in excitotoxic neuronal cell death that occurs in a variety of acute and chronic neurological disorders. The GluRs are categorized into two distinct classes, ionotropic and metabotropic receptors (Nakanishi, 1992; Seeburg, 1993). The ionotropic receptors (iGluRs) contain cation-specific ion channels, and are further subdivided into three groups: α -amino-3-hydroxy-5-methyl-4-isoxazolepropionate (AMPA), kainate and N-methyl-D-aspartate (NMDA) receptor channels according to their selective agonists. On the other hand, the metabotropic receptors (mGluRs) are coupled to GTP-binding proteins (G-proteins) and modulate the production of intracellular messengers.

The NMDA receptors, one of the three major subtypes of ionotropic glutamate receptors, are highly permeable to Ca^{2+} and required for the induction of long-term potentiation (LTP) of synaptic efficacy, a form of activity-dependent synaptic plasticity of the hippocampus (Bear and Malenka, 1994; Sakimura et al., 1995; Kiyama et al., 1998; Sprengel et al., 1998; Nicoll and Malenka, 1999; Grosshans et al., 2002)

NMDA receptors are composed of seven known subunits- GluR ζ 1 (NR1), GluR ϵ 1-4 (NR2A-2D) and GluR χ 1-2 (NR3A-3B). The GluR ζ 1 subunit serves as a fundamental subunit necessary for formation of the NMDA receptor activities. Heteromeric assemblies of GluR ζ 1 with one or more other subunits confer the NMDA receptors distinct gating and ion conductance properties (Hollmann and Heinemann, 1994; Nakanishi and Masu, 1994; Dingledine et al., 1999).

The GluR ζ 1 subunit is expressed in vast majority of central neurons throughout all

developmental stages, whereas the GluR ϵ 1-4 subunits are expressed in neurons with distinct spatial and temporal patterns (Watanabe et al., 1992). For example, the GluR ζ 1 and GluR ϵ 1-2 subunit mRNAs are heavily expressed in the hippocampus, whereas the GluR ϵ 3-4 subunit mRNAs are not detected in the hippocampus throughout development (Watanabe et al., 1992, 1993). The GluR ϵ 2 subunit mRNA is expressed from the embryonic period to adulthood, whereas the GluR ϵ 1 subunit mRNA is not expressed during the embryonic stage, but appears at postnatal day 1 in the CA1 region of the hippocampus and strikingly increases in the entire brain during the first two weeks after birth (Watanabe et al., 1992).

Most neurons in the central nervous system receive excitatory inputs from several sources; meanwhile, single kind of excitatory input can also innervate several types of postsynaptic target cells. It was suggested that NMDA receptor subunit abundance was different not only in different brain regions but also in different synapses on the same cells in an input-selective manner in the hippocampus (Gottmann et al., 1997; Fritschy et al., 1998; Ito et al., 2000). It has been reported that ϵ 2 subunit contribution to synaptic NMDA response in pyramidal cells is asymmetrical between the left and right hippocampus and between the apical and basal dendrites of single pyramidal cells (Kawakami et al., 2003). In this study, it is also suggested that ϵ 2 subunit contribution is different between synapses on the same cells depending on the side of input origin (ipsilateral or contralateral CA3 pyramidal cells). However, it is not yet clear whether this asymmetry is also dependent on the types of postsynaptic cells. To further characterize this asymmetry, I investigated the ϵ 2 distribution in individual synapses made by single type of Schaffer collateral input on distinct postsynaptic targets, pyramidal cells and interneurons, in the left and right CA1 area by quantitative

postembedding immunogold labeling. This method has been successfully applied to compare GABA_A and ionotropic glutamate receptor contents of distinct synapse populations (Nusser et al., 1996; Nusser et al., 1998b; Takumi et al., 1999).

In wild type mice, the distinct amounts of $\epsilon 2$ on Sch-CA1 pyramidal cell synapses of the left and right hippocampus result in different inhibitory effect of Ro 25-6981, a $\epsilon 2$ -selective antagonist, on NMDA EPSCs. However, amplitude of NMDA EPSCs relative to that of non-NMDA EPSCs was the same between left and right Sch-CA1 pyramidal cell synapses, indicating the same amount of NMDA receptor channels in these synapses (Kawakami et al., 2003). This is probably due to the presence of $\epsilon 1$ subunit because at the age of 2 week, when $\epsilon 1$ subunit is not yet expressed in a level comparable to that of $\epsilon 2$ subunit, the asymmetrical $\epsilon 2$ allocation is directly reflected in different amplitudes of LTP between the left and right hippocampus (Kawakami et al., 2003).

The knockout technology has been used to facilitate understanding of the biological importance and enhance difference in abundance of distinct NMDA receptor subtypes. For example, $\epsilon 1$ knock-out (KO) mice have been used to identify different input specific $\epsilon 1$ and $\epsilon 2$ abundance in CA3 pyramidal neuron synapses (Ito et al., 1997; Ito et al., 2000). In $\epsilon 1$ KO mice, the NMDA receptor composition in the hippocampal CA1 pyramidal cell is simplified to $\zeta 1$ and $\epsilon 2$ subunits (Sakimura et al., 1995). The amount of the functional NMDA receptors is expected to be directly proportional to the amount of the $\epsilon 2$ subunit. This situation could facilitate the detection of difference in the $\epsilon 2$ immunoreactivity. Moreover, in $\epsilon 1$ KO mice, although the NMDA receptor channel current and LTP in the CA1 area were significantly reduced compared to wild type mice and spatial learning was moderately impaired (Sakimura et al., 1995), the

expression of mRNAs for other NMDA receptor channel subunits was not affected by the $\epsilon 1$ disruption. In addition, efficacy of excitatory transmission in hippocampal CA1 pyramidal neurons estimated by the input–output curve was indistinguishable between the mutant and wild type mouse, indicating the $\epsilon 1$ disruption did not apparently affect non-NMDA receptor-mediated transmission.

Therefore, in the present study I employed $\epsilon 1$ KO mice to facilitate the detection of different $\epsilon 2$ distribution in synapses made by Schaffer collateral terminals onto distinct postsynaptic target cells, pyramidal cells and interneurons, between the left and right hippocampus.

Materials and Methods:

VHCT operation GluR ϵ 1 subunit knock out mice (9-10 w, C57BL/6 genetic background, otherwise stated) were anesthetized by pentobarbital injection (60 mg/Kg i.p.) and held on a stereotaxic apparatus. A small piece of a razor blade (2.5 mm wide) was glued onto a rod that was clamped on a micromanipulator. From an opening made in the skull, 3 mm wide and 4 mm long including the bregma, the blade was inserted 4.0 mm vertically at the midline of the brain to transect the VHC. To avoid damage to the sagittal sinus, the blade was shifted 0.5 mm to the right and inserted 0.5 mm into the cerebral cortex, and then was returned to the midline position as the blade was lowered. After slowly removing the blade, a piece of skull was returned to the hole, and the scalp was closed with sutures. Animals that underwent this procedure were viable for over 3 months without apparent abnormalities. Mouse brains were removed 5 days after surgery, and 150 μ m thick coronal serial slices were cut at the VHC level for confirming the complete transection of commissural fibers. All experiments were performed in accordance with the guidelines of the Japanese Committee on Animal Experiment, Japan.

Tissue preparation for electron microscopy Five days after the VHCT operation, GluR ϵ 1 subunit knock out mice (9-10w, C57BL/6 genetic background) were anesthetized by pentobarbital (60 mg/kg, i.p.) and perfused with 25mM phosphate-buffered saline (PBS, pH 7.4) transcardially followed by fixative containing 4% paraformaldehyde, 0.05% glutaraldehyde and 0.5% picric acid in 0.1 M phosphate buffer (PB, pH 7.4) for 15 min. After perfusion, the brains were removed and 150 μ m thick coronal slices were cut through the VHC (bregma $-0.22 \sim -0.82$) for confirming the complete VHCT and 100 μ m and 350 μ m thick coronal slices were cut alternately

from left and right dorsal hippocampal CA1 region.

After washed in several changes of 0.1M PB, the 100 μ m slices were undergone postfixation in 1% osmium tetroxide in 0.1 mM PB, dehydration and then were flat embedded in Durcupan resin (ACM, Fluka, Switzerland) between liquid release-coated (MATSUNAMI GLASS IND., LTD, Japan) slides and cover slips. After capsule embedding of hippocampal CA1 region, blocks were trimmed and ribbons of serial 70nm-thick sections were collected on pioloform-coated single-slot grids, contrasted by uranyl acetate and lead citrate and examined using a JEOL 1200EX electron microscope.

The small tissue blocks cut from both sides of 350 μ m thick coronal slices of hippocampal CA1 region were cryoprotected in 10, 20, or 30% glycerol in 0.1mM PB, pH 7.4, overnight. They were then frozen by plunging into liquid propane (-185°C) cooled by liquid nitrogen rapidly in a cryofixation unit KF80 (Reichert, Vienna, Austria). Freeze-substitution and low-temperature embedding in Lowicryl HM20 were performed subsequently(Matsubara et al., 1996). Briefly, the samples were immersed in 1% uranyl acetate dissolved in anhydrous methanol (-90°C , 24 hr) in a cryosubstitution unit (AFS; Reichert). The temperature was raised in steps of $4^{\circ}\text{C}/\text{hr}$ from -90°C to -45°C . The samples were washed three times with anhydrous methanol and infiltrated with Lowicryl HM20 resin (Polysciences, Inc.,USA) at -45°C with a progressive increase in the ratio of resin to methanol. Polymerization was performed with ultraviolet light (360 nm) at -45°C for 24 hr, the temperature was raised in steps of $5^{\circ}\text{C}/\text{hr}$ from -45°C to 0°C during UV irradiation and polymerization was performed continuously at 0°C for 36hr. The polymerized samples were taken out of the mall and exposed to diffuse UV radiation for 1 day at room temperature.

Antibodies and controls in postembedding immunocytochemistry Polyclonal antibodies to synthetic peptides, corresponding to amino acid residues 1-48 and 1353-1432 of the mouse GluR ϵ 2 subunit were raised in rabbits and affinity purified as described by Watanabe et al. (1998). They recognized in immunoblots a single band at 180 kDa in membrane fractions prepared from newborn wild-type mouse brain. Immunoreactivity of the 180 kDa protein band disappeared in newborn GluR ϵ 2 (-/-) mice. The antibodies were referred to as anti-GluR ϵ 2N and anti-GluR ϵ 2C and were used at concentration of 10 μ g/ml. For GluR ϵ 2 labeling, sections were incubated in anti-GluR ϵ 2C (kindly provided by Dr. M. Watanabe) or mixed anti-GluR ϵ 2C and anti-GluR ϵ 2N (at 10 μ g ml⁻¹ respectively, kindly provided by Dr. M. Watanabe) to increase the labeling intensity for quantification. A polyclonal antibody to a synthetic peptide, corresponding to amino acid residues 909-938 of the C-terminal of the C2 cassette of mouse GluR ζ 1 was raised in rabbits and affinity purified as described by Yamada et al. (2001). This antibody (anti- GluR ζ 1C) recognized in immunoblot a single band at 120 kDa in membrane fraction prepared from adult mouse brain. The antibody was used at concentration of 10 μ g/ml. A polyclonal antibody to a synthetic peptide corresponding to amino acid residues 436-450 of the extracellular domain of all rat NR1 subunit splice forms was raised in rabbits and affinity purified as described by Pickard et al. (2000). This antibody (anti-GluR1 ζ 1N) recognized in immunoblot a single band at 115 kDa in NR1a-expressing COS-7 cells and in membrane fraction prepared from rat brain. The amino acid residues 436-450 of mouse were the same as those of rat. The antibody was used at concentration of 10 μ g/ml. For GluR ζ 1 labeling, sections were incubated in anti-GluR ζ 1C (kindly provided by Dr. M. Watanabe) or mixed anti-GluR ζ 1C and anti-GluR ζ 1N (kindly provided by Dr. E. Molnar) to increase the

labeling intensity for quantification of synaptic labeling. A commercial rabbit polyclonal antibody (CHEMICON International, Inc, catalog no.: AB1506) to a synthetic peptide, corresponding to amino acid residues 871-893 of the C-terminal rat GluR2, recognizing both GluR2 and GluR3 (Boulter et al., 1990) was also used at concentration of 5 ug/ml. This antibody has no cross-reactivity with GluR1 or GluR4 and was referred to as anti-GluR2/3. The GluR2 and GluR3 of mouse and rat have identical carboxy terminal sequences.

For GluR4 labeling, sections were incubated in mixed primary guinea pig polyclonal antibodies against GluR4C and GluR4N (at 10 $\mu\text{g ml}^{-1}$ respectively, kindly provided by Dr. M. Watanabe). Anti-GluR4C and anti-GluR4N was raised in guinea pigs to residues 861-881 of the C terminal and residues 262-294aa of the N terminal respectively.

All primary antibodies used except anti-GluR4 were affinity purified and extensively tested for their specificity as described (Yamada et al., 2001; Pickard et al., 2000; Watanabe et al., 1998). After omitting each of these antibodies, immunoreactivity for the respective subunit was not detected.

Postembedding immunocytochemistry The similar procedure was used as described earlier (Nusser et al., 1998a). To ensure the same incubation condition, Lowicryl-embedded ultrathin sections (85 nm thickness) from the both sides of the CA1 subfield were picked up onto the same nickel 400 mesh grids that had been coated with coat-quick "G" medium (Daido Sangyo Company, Japan) to prevent the detachment of the sections during processing. Then the sections were treated with a saturated solution of NaOH in 100% ethanol for 2 sec. After being washed, the sections were incubated in

blocking solution (2 % human albumin serums in TBS with 0.1 % Triton X-100) for 30 min, followed by incubation with the primary antibodies (diluted in blocking solution) overnight at room temperature. After several washes with TBS for 30 min, the sections were incubated in the secondary antibody (anti-rabbit IgG tagged with 5 nm colloidal gold, British Biocell International, Cardiff, UK) diluted (1:100) in blocking solution-containing polyethyleneglycol (5 mg ml⁻¹) for 3 hr. Incubations in secondary antibodies were followed by washing in ultra pure water. Then the sections were contrasted with saturated aqueous uranyl acetate and then with lead citrate. After washing and drying, sections were examined with JEOL 1200EX electron microscope.

Double-labeling postembedding immunocytochemistry Ultrathin sections (85 nm thickness) picked up onto the coat-quick "G" medium coated nickel 400 mesh grids were reacted as described above. To avoid the attenuation of the $\epsilon 2$ signal, I adopted a sequential application of the anti- $\epsilon 2$ and anti-GluR $\alpha 4$ antibodies. Briefly, by incubation with the anti- $\epsilon 2$ primary antibodies for 10 hr at room temperature and several washes with TBS for 30 min, the sections were incubated in the secondary antibody (anti-rabbit IgGs tagged with 5 nm colloidal gold, British Biocell International, Cardiff, UK) diluted (1:100) in blocking solution-containing polyethyleneglycol (5 mg ml⁻¹) for 3 hr. After several washes with TBS for 30 min, the sections were incubated in the anti-GluR $\alpha 4$ primary antibodies overnight at room temperature followed by several washes with TBS for 30 min and incubation in the secondary antibody (anti-guinea pig IgGs tagged with 10 nm colloidal gold, British Biocell International, Cardiff, UK) diluted (1:100) in blocking solution-containing polyethyleneglycol (5 mg ml⁻¹) for 3 hr. Incubations in secondary antibodies were followed by washing in ultra pure water. Then the sections

were contrasted with saturated aqueous uranyl acetate, followed by lead citrate. After washing and drying, sections were examined with a JEOL 1200EX electron microscope.

Quantification of postembedding immunogold labeling Electron micrographs with a final magnification of $25000 \times$ were obtained at random from the middle parts of the stratum radiatum and stratum oriens of CA1 region. For quantification on excitatory synapse from pyramidal cell, all asymmetrical axospinous synapses with distinct postsynaptic density (PSD), synaptic cleft, and presynaptic membrane were subjected to quantification of immunoparticle number per unit length of PSD (particles/ μm). It cannot be excluded that a small proportion of postsynaptic profiles classified here as dendritic spines were, in fact, thin dendritic shafts lacking mitochondria in the examined segment. I consider their contribution to the population of spine synapses to be minor on the basis of the low proportion of interneurons and the lower number of synapses per interneuron, as compared with pyramidal cells. For quantification on excitatory synapse from GluR4-negative interneurons, asymmetrical synapses with synaptic cleft, presynaptic membrane and distinct PSD from the dendritic shafts and dendrites containing mitochondria and without 10nm GluR4 labeling were subjected to quantification of 5nm $\epsilon 2$ immunoparticle number per unit length of PSD (particles/ μm). For quantification on excitatory synapse from GluR4-positive interneurons, asymmetrical synapses with synaptic cleft, presynaptic membrane and distinct PSD from the dendritic shafts and dendrites containing mitochondria and with at least 2 10nm GluR $\alpha 4$ immunogold particles on the synapses were subjected to quantification of 5nm $\epsilon 2$ immunoparticle number per unit length of PSD (particles/ μm). Particles were included only if their centers were projected within 30nm of the inner leaflet of the

postsynaptic membrane and within the 30nm of the lateral edge of the PSD. The length of the PSD was measured by using the Scion Image software (Scion corporation, USA). Blind comparisons of immunogold particle density were made between the left and right hippocampus for every experimental pair. No significant difference in average lengths of PSD between left and right hippocampus of each pair was regarded as a precondition of the density comparison. All data were expressed as mean \pm sem. I used Shapiro-Wilks test for determining the normality of the distribution of data in each animal group. The Kolmogorov-Smirnov test and Mann-Whitney *U* test was used to determine the significance of different distribution and mean values between the left and right hippocampus in each animal respectively. The Student's *t*-test was used to determine the significance of differences of the mean values between the two data groups. A level of confidence of $P < 0.05$ was adopted for statistical significance.

Animals for immunofluorescence labeling The brains of C57BL/6 mice (9-10w) were used for immunohistochemical analyses. Under deep pentobarbital anesthesia (100 mg/kg of body weight, i.p.), brains were fixed transcardially with 4% paraformaldehyde in 0.1 M sodium phosphate buffer (pH 7.2)

Antibodies and controls in double-immunofluorescence labeling A commercial mouse monoclonal antibody (Sigma, product no: P-3171) to parvalbumin was used at final dilution of 1:1000. It has been used in previous immunochemical study (Liu et al., 2003). A polyclonal antibody to a fusion protein containing C-terminal amino acid residues 859-1199 of the rat mGluR1 α were raised in rabbits and affinity purified (Shigemoto et al., 1997). It recognized in immunoblots a single band at 145 kDa in membrane fraction prepared from rat hippocampus. The amino acid sequence used for

the antibody production is nearly identical between rat and mouse mGluR1 α . This antibody was used at concentration of 2 $\mu\text{g/ml}$. A commercial rabbit polyclonal antiserum (Swant, code No: CB-38) to Calbindin D-28k was raised against recombinant rat calbindinD-28k. The amino acid sequence is nearly identical between rat and mouse Calbindin D-28k. It was used at dilution of 1:4000. A commercial rabbit polyclonal antibody (Chemicon, catalog No.: AB5054) to calretinin was raised against recombinant rat calretinin. It has been used in previous immunochemical study (Liu et al., 2003). The amino acid sequence is nearly identical between rat and mouse calretinin. It was used at dilution of 1:1000. For GluR4 labeling, sections were incubated in anti-GluR4N or anti- GluR4C (both at 2 $\mu\text{g ml}^{-1}$, kindly provided by Dr. M. Watanabe). GluR4N was raised in guinea pigs to residues 262-294aa residues of the N terminal. Polyclonal antibodies to a polypeptide, corresponding to C-terminal residues 828-881 of the mouse GluR α 4 was raised in rabbits and affinity purified as described (Hashimoto et al., 1999). It recognized in immunoblot a single band at 102 kDa in membrane fraction prepared from mouse cerebellum. The antibody was used at concentration of 10 $\mu\text{g/ml}$.

All polyclonal primary antibodies were affinity purified and extensively tested for their specificity as described. After omitting each of the primary antibodies, immunoreactivity for the respective protein was not detected.

Double-immunofluorescence staining All immunohistochemical reactions were performed at room temperature. Paraffin sections (5 μm) cut with a sliding microtome (Leica SM2000R, Nussloch, Germany) were mounted on glass slides coated with 3-aminopropyltriethoxysilane. Paraffin sections were incubated with 10% normal goat serum for 20 minutes. For parvalbumin protein, mGluR1 α , calbindin, calretinin and

GluR4 double staining, before the pepsin treatment, sections were incubated in primary monoclonal mouse antibodies against the parvalbumin protein, primary polyclonal rabbit antibodies against mGluR1 α , calbindin, or calretinin diluted in Tris saline (pH 7.4) containing 2% normal serum and 0.2% triton X-100 overnight, Alexa fluorescein 488-labeled goat anti-mouse IgG (H+L) (1:200, Molecular Probes, Inc.) or Alexa fluorescein 488-labeled goat anti-rabbit IgG (H+L) (1:200, Molecular Probes, Inc.) for 2 hr. After acquiring the images as 3 time-scanned section in the X-Y plane using a confocal laser-scanning microscope (Fluoview, Olympus), the microslicer sections were further processed for the second immunoreaction. I pretreated the sections with pepsin prior to the second immunohistochemical incubation. Before pepsin pretreatment, 0.2 N HCl was warmed up to 37°C in a water bath. Frozen aliquots containing 1ml pepsin solution (100 mg/ml) were thawed just before use, and added to 100 ml 0.2 N HCl solution. Then, sections prewarmed at 37°C in distilled water were transferred to the pepsin/HCl solution. After a given incubation time of 8 minutes, sections were briefly washed with phosphate-buffered saline (PBS, pH 7.2), and processed for the second immunoreaction. Pepsin-digested microslicer sections were incubated overnight with primary guinea pig antibodies against GluR4N, and then with Alexa fluorescein 594-labeled goat anti-guinea pig IgG (H+L) (1:200, Molecular Probes, Inc.) for 2 hr. Images were acquired again as three time-scanned section in the X-Y plane using a confocal laser-scanning microscope (Fluoview, Olympus). The overlapped images of respective double staining were got by Adobe photoshop 6.0 software.

After omitting the primary antibodies, immunoreactivity could not be detected (data not shown).

Quantitative analysis of adjacent sections This method requires the use of two adjacent (serial) sections. In the present experiment, 2 adjacent pairs were selected at random from the ribbon of serial sections of each group and were photographed by taking serials of micrographs without overlapping in each section. Electron micrographs were obtained at random from middle part of the stratum radiatum of CA1 of the dorsal hippocampus (about bregma -1.94mm) (Franklin et al, 1997). The same area was photographed from each section at a magnification of $\times 15000$. Photographs, with an area of about $500\ \mu\text{m}^2$, were assembled for each section area. Synapse profiles on spines were identified by the presence of at least three synaptic vesicles within the presynaptic bouton, a PSD within the postsynaptic bouton, a visible synaptic cleft and alignment of the pre and postsynaptic membranes. Synaptic densities were evaluated according to the formula;

$$N_V = \Sigma Q_{-} / V_{\text{dis}}$$

where ΣQ_{-} represented the number of synaptic profiles present in the test section and disappeared in the corresponding area of adjacent section, and which are not intersected by both of the two exclusion lines. V_{dis} was the volume of the test section, which was the area studied in the test section multiplied by the section thickness. (Calverley and Jones, 1987). The area studied was measured by using the Scion Image software (Scion corporation, USA). The analysis was performed in a double-blind fashion on electron micrographs from mice of different experimental treatments.

There were three mice in each experimental group and a block from left and right CA1 region respectively per animal was counted. The Student's *t*-test was used to determine the significance of differences between the mean values of data groups. A level of confidence of $P < 0.05$ was adopted for statistical significance.

Electrophysiology Transverse hippocampal slices (450 μm thick) were cut with a vibrating microtome (VT 1000 S) in ice-cold artificial cerebrospinal fluid (ACSF) (in mM: NaCl, 119; KCl, 2.5; CaCl₂, 2.5; MgSO₄, 1.3; NaH₂PO₄, 1.0; NaHCO₃, 26; glucose, 10, saturated with 95% O₂ / 5% CO₂). A mouse brain was fixed on an agar block, which was made by 2 pieces of agar slopes (with a slope of 20°) stuck together at a right angle, and mounted on the cutting stage. We lowered the left-rear or right-rear of the brain using agar slopes when we cut the left or right brain, respectively. Slices from a similar septotemporal level of the left and right hippocampus were used for experiments. Recordings were made in a submerged slice chamber perfused with ACSF at room temperature. Electrodes filled with 0.9 % NaCl were used for extracellular recording. Synaptic responses were evoked at 0.1 Hz using a bipolar tungsten electrode. An LTP-inducing tetanic stimulus was given at 100 Hz for 1 s at baseline stimulus strength. LTPs of the fEPSP slope were expressed as a percentage of the mean before tetanic stimulation. Synaptic currents were recorded from CA1 pyramidal neurons using the blind-patch technique in the whole-cell voltage-clamp mode (Axopatch 1D). A high-Mg²⁺ and Ca²⁺ (4 mM of MgSO₄ and CaCl₂) ACSF was used to increase membrane stability in the presence of bicuculline. Patch electrodes (3-5 M Ω) were filled with an intracellular solution (in mM: cesium gluconate, 122.5; CsCl, 17.5; HEPES buffer, 10; EGTA, 0.2; NaCl, 8; Mg-ATP, 2; Na₃-GTP, 0.3; pH 7.2). We recorded NMDA-EPSCs at +30 mV in the presence of DNQX (20 μM) and bicuculline (30 μM). Non-NMDA-EPSCs were recorded at -90 mV in the presence of bicuculline (30 μM). Series resistance (10-30 M Ω) was regularly monitored during recordings, and cells were rejected if more than a 20% change occurred during the experiment. All

records were filtered at 2 kHz, digitized at 4 kHz and stored on a computer equipped with an A/D converter (Mac Lab 2e). No failure was detected in our experiments. All data were expressed as a mean \pm sem and analyzed with Student's *t*-test.

Results:

Reduction of synapse density after VHCT operation

In order to examine synapses made by ipsilateral Sch fibers selectively, I transected the ventral hippocampal commissure (VHCT operation) 5 days prior to perfusion fixation (Kawakami et al., 2003). At 5 days after VHCT, reactive synaptogenesis should still be very slight (Steward et al, 1983). To confirm if the operation successfully eliminated synapses made by commissural afferents, I first examined density of intact synaptic profiles in a middle part of the CA1 stratum radiatum in naïve and VHCT-operated $\epsilon 1$ KO mice. In naïve $\epsilon 1$ KO mice, normal axospinous asymmetrical synapses were observed in the CA1 stratum radiatum (Fig. 1A). In VHCT-operated mice, typical electron-dense type degeneration was also observed in fiber terminals in the CA1 stratum radiatum (Fig. 1B). The mean density of intact axospinous asymmetrical synapses was significantly reduced ($n=3$, student t -test $P<0.05$) by 40% after VHCT operation, indicating that the majority of remaining synapses was Sch-CA1 pyramidal cell synapses. No significant difference in synapse density was detected between the left and right stratum radiatum in naïve ($1.61 \pm 0.09/\mu\text{m}^3$ and $1.63 \pm 0.05/\mu\text{m}^3$ respectively, $n=3$, t -test $P>0.05$, Fig. 1C) and VHCT-operated ($1.01 \pm 0.01/\mu\text{m}^3$ and $0.99 \pm 0.05/\mu\text{m}^3$, $n=3$ animals, student t -test $P>0.05$, Fig. 1C) mice. Moreover, the reduction rates were not significantly different between left and right stratum radiatum, indicating that the VHCT operation selectively denervates commissure fibers to an equivalent extent in the left and right CA1 area.

Asymmetry of $\epsilon 2$ subunit anatomical distribution between left and right Sch-CA1

pyramidal cell synapses

After confirming a complete transection of the VHC, I compared the distribution of $\epsilon 2$ subunit in Sch-CA1 pyramidal cell spines between the left and right hippocampus using postembedding immunogold labeling. EM examination showed strong gold particle labeling for $\epsilon 2$ in type 1 axospinous postsynaptic membrane specialization of the pyramidal cells in the stratum radiatum of the CA1 area in naïve and VHCT-operated wild-type and $\epsilon 1$ KO mice (Fig. 2A, 2B).

Density of immunoparticles was calculated by dividing number of particles over synapses (within 30nm from postsynaptic membrane) by length of the postsynaptic density in individual synaptic profiles. The mean immunoparticle density for $\epsilon 2$ was not significantly different in Sch-CA1 pyramidal cell synapses between the left and right hippocampus in wild type mice (Man-Whitney *U* test, $P > 0.05$ in all animals; Paired *t*-test, $P > 0.05$, in stratum radiatum, $n = 4$, Table 1). In wild type mice, in spite of the asymmetrical blocking effects of a $\epsilon 2$ -selective antagonist on NMDA EPSCs, the amplitude of NMDA EPSCs relative to that of non-NMDA EPSCs was not significantly different between left and right Sch-CA1 pyramidal cell synapses, indicating the same NMDA receptor content in these synapses (Kawakami et al., 2003). This result implies that $\epsilon 1$ subunits compensate for the difference in $\epsilon 2$ subunits in wild-type mice to get the same number of NMDA receptors between the left and right. In such a situation, only the number of $\epsilon 2$ subunits per one NMDA receptor but not the number of NMDA receptors is different between the left and right. Postembedding immunogold labeling method may not be sensitive enough to detect such difference in subunit composition because of steric hindrance; two immunogold particles for $\epsilon 2$ would not bind one NMDA receptor complex containing two $\epsilon 2$ subunits due to a short distance between

the subunits compared to the size of the antibody. In $\epsilon 1$ KO mice, subunit composition of NMDA receptors in CA1 pyramidal cells is simplified to $\zeta 1$ and $\epsilon 2$ (Sakimura et al., 1995). The amount of the functional NMDA receptors is expected to be directly proportional to the amount of $\epsilon 2$ subunits, which could be expected to facilitate the detection of difference in the $\epsilon 2$ immunoreactivity. Thus, I examined distribution of $\epsilon 2$ labeling in $\epsilon 1$ KO mice in the following study.

In naïve $\epsilon 1$ KO mice, the mean immunoparticle density for $\epsilon 2$ was not significantly different between the left and right stratum oriens and stratum radiatum (mouse 5, 6, 7, Man-Whitney U test, $P > 0.05$, in all animals; Paired t -test, $P > 0.05$, in stratum radiatum, $n = 3$, Table 2). However, in VHCT-operated $\epsilon 1$ KO mice, the density of immunoparticles for $\epsilon 2$ in the right stratum oriens was significantly higher than that in the left stratum oriens (mouse 1,2,4, Man-Whitney U test, $P < 0.05$, in all animals; Paired t -test, $P < 0.05$, $n = 3$, Table 2); whereas in the stratum radiatum, an opposite asymmetry was observed: the mean density for $\epsilon 2$ labeling in the left side was significantly higher than that in the right side (mouse 1,2,3,4, Man-Whitney U test, $P < 0.05$, in all animals; Paired t -test, $P < 0.05$, $n = 4$, Table 2). The mean ratio of $\epsilon 2$ labeling density in the left to right was about 1:1.5 in the stratum oriens and about 1.6: 1 in the stratum radiatum($n = 3$ and 4 respectively, Paired t -test, $P < 0.05$, Fig. 7). Distribution of immunoparticle density for $\epsilon 2$ in synaptic profiles was all positively skewed toward larger value (Shapiro-Wilk test, $P < 0.001$, shown for mouse 1 in Fig.3A, B). In mouse 1, the $\epsilon 2$ labeling density showed a significant difference in distribution (Kolmogorov-Smirnov test, $P < 0.05$) between the left and right with opposite directions in the stratum oriens and stratum radiatum (Fig.3A, B). The cumulative probability curves in the right stratum oriens and left stratum radiatum were shifted to right compared with those in the left stratum oriens and

right stratum radiatum respectively (shown for mouse 1 in Fig.3C, D). Similar results were obtained from other mice for the stratum oriens (mouse 2, 4) and stratum radiatum (mouse 2,3,4) respectively.

Moreover, in VHCT-operated $\epsilon 1$ KO mice, labeling density for $\epsilon 2$ was significantly different between basal and apical dendrites. The density of immunoparticles for $\epsilon 2$ in the right basal dendrites was significantly higher than that in the right apical dendrites (mouse 1,2,4, Man-Whitney *U* test, $P < 0.05$, in all animals, Table 2); whereas in the left hippocampus, an opposite asymmetry was observed: the mean density for $\epsilon 2$ labeling in the apical dendrites was significantly higher than that in the basal dendrites (mouse 1,2,4, Man-Whitney *U* test, $P < 0.05$, in all animals, Table 2). The mean ratio of $\epsilon 2$ labeling density in the basal to apical dendrites was about 1:1.4 in the left hippocampus and about 1.5:1 in the right hippocampus ($n=3$). Moreover, the $\epsilon 2$ labeling density distribution showed a significant difference (Kolmogorov-Smirnov test, $P < 0.05$) between the basal and apical dendrites with opposite directions in the left and right hippocampus. The cumulative probability curves in the right basal dendrites and left apical dendrites were shifted to right compared with those in the right apical dendrites and left basal dendrites respectively (shown for mouse 1 in Fig.3E, F). Similar results were obtained from other mice (mouse 2, 4).

As a control experiment, ultrathin sections from the same blocks were also reacted with an antibody to AMPA receptor subunits GluR2/3 in the CA1 stratum radiatum (mouse 4, Fig. 2C). Most of the spine synapses (81.6% in mouse 4) were immunopositive for GluR2/3, being consistent with previous postembedding immunogold labeling studies in the rat (Nusser et al., 1998b). In contrast to the asymmetrical distribution of $\epsilon 2$ labeling, immunoparticle density in pyramidal cell

synapses for GluR2/3 was not significantly different between the left and right CA1 stratum radiatum in both naïve mice (mouse 5, 6, Man-Whitney U test, $P > 0.05$ in all animals, Table 2) and VHCT-operated $\epsilon 1$ KO mice (mouse 1, 2, 3, 4, Man-Whitney U test, $P > 0.05$ in all animals; Paired t -test $P > 0.05$, $n=4$, Table 2). Left/right ratios of GluR2/3 immunoparticle density in the stratum radiatum were calculated and averaged. The mean ratio for GluR2/3 in Sch-CA1 pyramidal cell synapses was 0.94 ± 0.06 ($n=4$, not significantly different from 1.0, paired t -test $P > 0.05$, Fig.7), indicating comparable efficiency of immunoreaction between the paired blocks.

$\zeta 1$ subunit distribution between left and right Sch-CA1 pyramidal cell synapses

Since functional activities of the NMDA receptor channel require the heteromeric assembly of $\zeta 1$ subunits with $\epsilon 2$ subunits, I next compared the $\zeta 1$ distribution between the left and right Sch-CA1 pyramidal cell synapses in the $\epsilon 1$ KO mice.

Most of the asymmetrical synapses (83.2% in mouse 1) in the stratum radiatum of the CA1 area were immunopositive for an antibody to all $\zeta 1$ splice forms in the CA1 area (mouse 1, Fig.2D), being consistent with previous postembedding immunogold-labeling studies in the rat (Nyiri et al., 2003). In naïve $\epsilon 1$ KO mice, the mean immunoparticle density for $\zeta 1$ in Sch-CA1 pyramidal cell synapses was not significantly different between the left and right stratum radiatum (mouse 5,6, Man-Whitney U test, $P > 0.05$, Table 2). In VHCT operated $\epsilon 1$ KO mice, the $\zeta 1$ labeling density in these synapses was also not significantly different between the left and right stratum radiatum (mouse 1, 2, 4, Man-Whitney U test, $P > 0.05$, Table 2) except one animal (mouse 3, Man-Whitney U test, $P < 0.05$, Table 2). Left/right ratios of $\zeta 1$ immunoparticle density in the stratum radiatum were calculated and averaged. The mean ratio for $\zeta 1$ in Sch-CA1 pyramidal cell

synapses was 1.13 ± 0.18 (n=4, not significantly different from 1.0, paired *t*-test $P > 0.05$, Fig. 7), indicating comparable $\zeta 1$ immunoparticle density between the left and right hippocampus.

Distribution of GluR4 in parvalbumin (PV) - and mGluR1 α -positive interneurons in CA1

To further elucidate whether this asymmetrical $\varepsilon 2$ distribution is dependent on types of postsynaptic cells, I investigated the $\varepsilon 2$ distribution in Sch-interneuron synapses. Interneurons in the hippocampus possess a rich diversity and include multiple populations. Since one of the AMPA receptor subunits, GluR4, is strongly expressed in some interneurons but not in pyramidal cells in the rat hippocampus (Catania et al., 1998), I examined the $\varepsilon 2$ distribution in synapses on GluR4-positive and negative interneuron dendrites.

Firstly, I used double immunofluorescence staining to identify the GluR4-positive interneurons. Cell bodies of the GluR4-immunopositive interneurons were mainly localized in the stratum pyramidale, stratum oriens and adjoining alveus. GluR4-immunoreactive interneurons were rare in the stratum radiatum (1 in 62, in 2 animals). The GluR4-immunoreactivity was also localized to radically oriented dendrites of interneurons in both strata oriens and radiatum of the CA1 area. The pyramidal cells were immunonegative for GluR4 (Fig. 4A1). Some interneuron somata, mostly in and near the pyramidal cell layer, were strongly immunopositive for PV (Fig. 4A2). Double immunofluorescence staining revealed an extensive overlap of GluR4- and PV- immunoreactive neurons (Fig. 4A3). Most of the GluR4-immunopositive interneurons were PV immunoreactive (55 in 62, 88.7%) and all PV-immunoreactive

interneurons were GluR4 immunopositive (55 in 55, 100%).

One of the alternatively spliced isoforms of metabotropic glutamate receptor subtype 1 (mGluR1 α) is particularly rich in O-LM interneurons (Ferraguti et al., 2004). Immunofluorescence showed strongly mGluR1 α immunopositive cell bodies and dendrites, mainly in the alveus and adjoining stratum oriens in the CA1 area (Fig. 4B2), being coincident with previous studies in the rat (Baude et al., 1993; Losonczy et al., 2002; Ferraguti et al., 2004). Similar to the distribution pattern of mGluR1 α -immunopositive interneurons, some interneuron soma and their numerous dendrites in the stratum oriens or alveus were GluR4-immunopositive (Fig. 4B1). Double immunofluorescence showed that 11.1% (10 in 90) of GluR4-immunopositive interneurons were immunoreactivity for mGluR1 α , and 35.9% (14 in 39) of mGluR1 α -immunopositive interneurons were immunoreactivity for GluR4 (Fig. 4B3) in the strata pyramidale and oriens, and alveus. Therefore, not only PV-immunoreactive interneurons, but also a small population of mGluR1 α - immunoreactive interneurons are included in the GluR4-immunopositive interneurons.

Absence of immunoreactivity for GluR4 in Calbindin and Calretinin immunoreactive interneurons in CA1

Three kinds of calcium binding proteins, PV, calbindin (CB) and calretinin (CR) represent non-overlapping populations of GABAergic cells in the hippocampus (Miettinen et al., 1992). I also investigated GluR4 immunoreactivity in CB- and CR-positive interneurons.

Both CB- and CR- positive neurons were localized in all layers of the CA1 area, but they exhibited a slightly different distribution. Strongly CB-immunopositive neurons

were present mostly in distal one-third of the stratum radiatum and some superficially located pyramidal cells also weakly expressed CB. CR-immunopositive interneurons were also frequently found in the stratum pyramidale, being consistent with earlier studies (Sloviter, 1989; Gulyas et al., 1996) (Fig5. A2, B2). However, almost all of the GluR4-immunopositive interneurons were present in the stratum pyramidale (Fig. 5A1, A2).

Double immunofluorescence showed that neither CB-immunopositive interneurons (17 counted) nor CR-immunopositive interneurons (26 counted) were immunoreactive for GluR4 (Fig. 5A3, B3).

No asymmetry of $\epsilon 2$ subunit distribution between left and right Sch-CA1 interneuron synapses

In the hippocampal CA1 area, besides pyramidal cells, interneurons also receive excitatory inputs from Schaffer collateral fibers on their dendritic shafts (Gulyas et al., 1999). Glutamatergic synaptic neurotransmission in these synapses is mostly mediated by AMPA and NMDA type glutamate receptors. After identification of the GluR4-immunopositive and GluR4-immunonegative interneurons, $\epsilon 2$ distribution in these two populations of Sch-CA1 interneuron synapses was investigated in CA1 stratum radiatum.

EM examination revealed strong 5nm particle labeling for $\epsilon 2$ in type 1 synapses on dendritic shafts (Fig. 6A, B and C), being in line with previous results (Racca et al., 2000). Moderate 10 nm particle labeling for GluR4 was also found in type 1 synapses on dendritic shafts (Fig. 6C).

In VHCT-operated $\epsilon 1$ KO mice, the mean immunoparticle density for $\epsilon 2$ was not

significantly different between left and right Sch-CA1 interneuron synapses for both GluR4-positive and GluR4-negative interneurons (mouse1, 2, 3, Man-Whitney U test $P > 0.05$, in all animals, paired t -test $P > 0.05$, $n=3$, Table 3). Left/right ratios of immunoparticle density for $\epsilon 2$ in the stratum radiatum were calculated and averaged in GluR4-positive and GluR4-negative interneurons. Mean ratios for $\epsilon 2$ on GluR4-positive interneuron synapses and GluR4-negative interneuron synapses were 0.88 ± 0.04 and 1.14 ± 0.12 ($n=3$, not significantly different from 1.0, paired t -test $P > 0.05$ respectively, Fig.7), indicating comparable $\epsilon 2$ immunoparticle density between the left and right Sch-CA1 GluR4-positive and GluR4-negative interneuron synapses respectively. In addition, after pooling the data for $\epsilon 2$ density in left and right interneuron synapses, mean density value in GluR4-positive interneuron synapses (8.88 ± 2.65 particles/ μm , $n=105$) was significantly lower (paired t -test $P < 0.01$) than that in GluR4-negative interneuron synapses (25.23 ± 3.80 particles/ μm , $n=138$).

Asymmetry of NMDA EPSCs between left and right Sch-CA1 synapses in $\epsilon 1$ KO VHCT mice

We further characterized NMDA-EPSCs at the CA1 pyramidal neuron synapses in the slices prepared from Wild type (WT) VHCT operated mice and $\epsilon 1$ KO VHCT operated mice. To record NMDA-EPSCs, whole-cell patch-clamp recordings were made from CA1 pyramidal neurons in the presence of 6,7-dinitroquinoxaline-2, 3-dione (DNQX, 20 μM) and bicuculline (30 μM) at a holding potential of +30 mV. Since excitatory synapses on CA1 pyramidal neurons localized on both apical and basal dendrites, NMDA-EPSCs were independently elicited by electrical stimuli applied

either at the stratum oriens (basal dendritic synapses) or at the stratum radiatum (apical dendritic synapses) of area CA1.

Fig. 8A illustrates the results obtained with the stimulation at basal dendritic synapses. In WT VHCT operated mice, stimulating the Schaffer collateral fibers to CA1 str. oriens elicited NMDA-EPSCs with similar amplitude (WT, Fig. 8A, left, middle panel). The NMDA-EPSCs component evaluated by the NMDA/non-NMDA EPSC ratios and evoked at the same stimulation intensity, were indistinguishable between left and right side VHCT mice slices (left basal, $57.4\% \pm 7.32$, $n = 5$, from 5 animals; right basal, $64.4\% \pm 5.66$, $n = 5$, from 5 animals; $P > 0.05$, t -test) (WT, Fig. 8A, right). By contrast, in $\epsilon 1$ KO VHCT operated mice, stimulating the Schaffer collateral fibers to CA1 str. oriens elicited NMDA-EPSCs with different amplitude (Fig. 8A, left, lower panel). The amplitude ratios of NMDA EPSCs to DNQX-sensitive non-NMDA EPSCs, evoked at the same stimulation intensity, were larger in the right hippocampal slices than in the left side (left basal, $21.6\% \pm 2.64$, $n = 5$ from 5 animals; right basal, $40.2\% \pm 3.40$, $n = 5$, from 5 animals; $P < 0.01$, t -test) ($\epsilon 1$ (-/-), Fig. 8A, right). Perforant path (pp) fibers from entorhinal cortex form synapses on CA1 pyramidal neurons in the stratum lacunosum moleculare (Amaral et al, 1995) and pp-CA1 synaptic responses were suppressed by the activation of presynaptic group II metabotropic glutamate receptors (mGluRs) expressed in these fibers (Petralia et al., 1996; Shigemoto et al., 1997; Kilbride et al., 1998; Contractor et al., 2000). Application of the group II selective mGluR agonist L-CCG-1 ($20 \mu\text{M}$) did not depress EPSCs evoked by stimulation at the stratum radiatum of area CA1 ($102 \pm 7\%$ of control, $n = 5$ from 5 animals), verifying that the currents were not contaminated by pp inputs.

An opposite asymmetrical effect was observed in response to stimulation at the stratum radiatum (Fig. 8B). In WT VHCT operated mice, stimulating the Schaffer collateral fibers to CA1 stratum radiatum elicited NMDA-EPSCs with similar amplitude (Fig. 8B, left, middle panel). The amplitude ratios of NMDA EPSCs to DNQX-sensitive non-NMDA EPSCs, evoked at the same stimulation intensity, were indistinguishable between left and right side VHCT mice slices (left apical, $61.6\% \pm 7.36$, $n = 5$, from 5 animals; right apical, $61.2\% \pm 3.89$, $n = 5$, from 5 animals; $P > 0.05$, t -test) (WT, Fig. 8B, right). By contrast, in $\epsilon 1$ KO VHCT operated mice, stimulating the Schaffer collateral fibers to CA1 stratum radiatum elicited NMDA-EPSCs with mirror-image asymmetry of that found in stratum oriens (Fig. 8B, left, lower panel). The amplitude ratios of NMDA EPSCs to DNQX-sensitive non-NMDA EPSCs, evoked at the same stimulation intensity, were larger in the left hippocampal slices than in the right side (left apical, $39.3\% \pm 3.40$, $n = 6$, from 6 animals; right apical, $16.4\% \pm 3.11$, $n = 5$, from 5 animals; $P < 0.01$, t -test) ($\epsilon 1$ (-/-), Fig. 8B, right). Since functional NMDA receptor complexes at synapses appeared to require both $\zeta 1$ and $\epsilon 2$ subunit proteins for full function, the asymmetrical NMDA EPSCs observed in the slice of $\epsilon 1$ KO VHCT operated mice not only revealed asymmetrical functional NMDA receptors content, but also directly reflected the asymmetrical functional $\epsilon 2$ subunit content on Schaffer collateral-CA1 (Sch-CA1) synapses between the left and right hippocampus.

Asymmetry in LTP

NMDA receptors mediated associative activity-dependent changes in synaptic efficacy including long time potentiation (LTP) of transmission in the hippocampus. The asymmetrical $\epsilon 2$ content was directly reflected in different amplitudes of LTP in $\epsilon 1$ KO

VHCT operated mice. In the left Sch-CA1 synapse, the amplitudes of LTP were similar between WT and $\epsilon 1$ KO mice. (WT mice, $153\% \pm 4.70$, $n = 6$ from 6 animals; $\epsilon 1$ KO mice, $138\% \pm 2.76$, $n = 7$, from 7 animals, $P > 0.01$, Fig. 9 left). In the right Sch-CA1 synapse, however, the amplitude of LTP in the $\epsilon 1$ KO mice was smaller than that in WT mice (WT mice, $150\% \pm 6.34$, $n = 5$, from 5 animals; $\epsilon 1$ KO mice, $104\% \pm 2.77$, $n = 6$, from 6 animals, $P < 0.01$, Fig. 9 right). The amplitude of LTP was higher in left Sch-CA1 synapses than that in the right Sch-CA1 synapses (left, $138\% \pm 2.76$, $n = 7$, from 7 animals; right, $104\% \pm 2.77$, $n = 6$, from 6 animals, $P < 0.05$, t -test), consistent with the larger degree of contribution of $\epsilon 2$ subunits to LTP in the left Sch-CA1 synapses.

Discussion:

Main conclusions of the present study are:

1. The density of $\epsilon 2$ subunit of NMDA receptor in Sch-CA1 pyramidal cell synapses is significantly different not only between the left and right hippocampus with opposite directions in the stratum radiatum and stratum oriens, but also between basal and apical dendrites with opposite directions in the left and right hippocampus.
2. The asymmetrical $\epsilon 2$ distribution is target-cell dependent. No asymmetrical $\epsilon 2$ distribution was detected in either Sch-GluR4-positive interneuron synapses or Sch-GluR4-negative interneuron synapses.
3. The asymmetrical $\epsilon 2$ distribution results in difference in amplitudes of NMDA EPSCs and LTP between the left and right hippocampus in $\epsilon 1$ knockout mice, indicating asymmetrical NMDA receptor content in Sch-CA1 pyramidal cell synapses.

Target-cell-specific asymmetry in $\epsilon 2$ allocation in synapses made by Schaffer collateral fibers in CA1 area

By quantitative immunogold labeling method, we detected asymmetrical $\epsilon 2$ distribution between left and right CA1 pyramidal cell spine synapses but not CA1 interneuron synapses in VHCT-operated $\epsilon 1$ KO mice, indicating a target-cell-specific asymmetry of $\epsilon 2$ allocation in synapses made by Sch fibers in CA1. Density of GluR2/3 subunit in Sch-CA1 pyramidal cell synapses was not significantly different between the left and right hippocampus in every animal examined, confirming similar sensitivity of the immunodetection between the paired blocks.

Unlike pyramidal cells, GABAergic interneurons possess a rich diversity and include multiple populations that could be distinguished on the basis of their morphological

features, neurochemical features, or intrinsic firing patterns (Freund and Buzsaki, 1996). In this study, we focused on two populations of Sch-CA1 interneuron synapses in the stratum radiatum, one on GluR4-positive interneuron dendritic shafts and the other on GluR4-negative interneuron dendritic shafts. Although we detected a significant difference in $\epsilon 2$ density between synapses on Sch-GluR4-positive and Sch-GluR4-negative interneurons, no left-right difference was found in either population of synapses. Immunogold labeling studies have confirmed the presence of NMDA receptors in synapses on CA1 interneuron dendrites with a polyclonal antibody that recognizes eight splice variants of the NR1 ($\zeta 1$) subunit (Nyiri et al., 2003), or with a mixture of antibodies to the NR1($\zeta 1$), NR2A($\epsilon 1$) and NR2B($\epsilon 2$)(Racca et al., 2000). In the present study, by using antibodies specific to the $\epsilon 2$ subunit, we showed that the mean $\epsilon 2$ immunoparticle density on GluR4-negative interneuron shafts was about 3 times as high as that on GluR4-positive interneuron shafts. Similarly, the mean $\zeta 1$ immunoparticle density on randomly found interneuron dendritic shafts was also about 3 times as high as that on PV-positive interneuron shafts in hippocampal CA1 area (Nyiri et al., 2003). The consistent low content of $\epsilon 2$ and $\zeta 1$ subunits in PV-immunoreactive neurons may cause their relative resistance to excitotoxic insults (Nitsch et al., 1989a,b).

Expression of synaptic receptors depends both on postsynaptic cell types receiving common afferents and different afferent types innervating common postsynaptic cells (Shigemoto et al., 1996; M.E. et al., 1997; Nusser et al., 1998b; Kumar et al., 2003). My study shows that, besides influencing the receptor content, the target cells also influence the left-right asymmetry of receptor distribution in synapses made by common afferents.

Identification of the GluR4-immunopositive interneurons and NMDA receptor subunit expression in hippocampal interneuron synapses

The GluR4 subunit has been suggested to be mainly expressed in hippocampal PV-positive interneurons with a very weak expression in pyramidal cells at the mRNA level (Geiger et al., 1995; Catania et al., 1998). Immunoreactivity for GluR4 was also observed in PV-containing interneurons in the hilus (Catania et al., 1998). Our double immunofluorescence staining showed that 88.7% percent of GluR4-positive interneurons were PV immunopositive and all PV-immunopositive interneurons were GluR4 immunopositive in the hippocampal CA1 area. Consistent with a previous report showing that the PV containing dendrites have a much higher synaptic coverage than other interneuron dendrites (Matyas et al., 2004), the GluR4-positive dendrites had a higher synaptic coverage than the GluR4-negative dendrites (Fig. 7C). At least 3 kinds of interneurons, basket cells, bistratified cells and axo-axonic cells express PV and extend their dendrites to the stratum radiatum in the hippocampus CA1 area (Oliva et al., 2000; Klausberger et al., 2003; Klausberger et al., 2004).

We found that a small proportion (11.1%) of the GluR4-positive interneurons express mGluR1 α in the stratum oriens. It is well known that O-LM interneurons, most of which were localized in the stratum oriens and adjoining alveus of CA1 area, have a strong immunoreactivity for mGluR1 α (Baude et al., 1993; Losonczy et al., 2002; Ferraguti et al., 2004). Also, some interneurons displayed weak to moderate mGluR1 α immunoreactivity, including interneuron-targeting interneurons (IS) in the strata pyramidale, radiatum, and lacunosum-moleculare, oriens-bistratified cells (O-Bi) in the stratum oriens, and a subpopulation of CCK-immunoreactive interneurons in the strata

pyramidale and radiatum (Losonczy et al., 2002; Ferraguti et al., 2004). Since the overlap occurred in the interneurons whose soma was localized in the stratum oriens and alveus in our study, we parsimoniously consider that some O-LM cells and O-Bi cells may contribute to a small subpopulation of GluR4-immunopositive dendrites in the CA1 stratum radiatum. On the other hand, the GluR4-immunonegative interneuron dendrites may at least originate from calretinin- and calbindin-containing interneurons, which also send their dendrites to the stratum radiatum (Freund and Buzsaki, 1996), as well as from interneurons that were unidentified in the present study.

Although I did not detect asymmetrical $\epsilon 2$ distribution between left and right Sch-CA1 interneuron synapses on either GluR4-immunopositive or GluR4-immunonegative interneuron dendrites, existence of asymmetrical $\epsilon 2$ distribution in some subpopulation(s) of interneurons could not totally be excluded. The diversity of the interneurons may hamper detection of the asymmetry in a small population of interneurons.

In situ hybridization studies suggested that $\zeta 1$, $\epsilon 1$ and $\epsilon 2$ mRNAs are dominant in hippocampal pyramidal cells. However, in several subsets of GABAergic interneurons, besides the dominant expression of $\zeta 1$, $\epsilon 1$, $\epsilon 2$ mRNA, $\epsilon 4$ mRNA is also weakly expressed (Watanabe et al., 1993; Monyer et al., 1994; Catania et al., 1996; Standaert et al., 1999). Synaptic immunolabeling for NMDA receptors on interneurons has been demonstrated only with a polyclonal antibody recognizing $\zeta 1$ (He et al., 1998), or with a mixture of antibodies to the $\zeta 1$, $\epsilon 1$ and $\epsilon 2$ (Racca et al., 2000). The $\zeta 1/\epsilon 4$ receptors activated and deactivated slowly, during seconds rather than hundreds of milliseconds, and are less sensitive to voltage-dependent Mg^{2+} block than $\zeta 1/\epsilon 1$ or $\zeta 1/\epsilon 2$ receptors (Monyer et al., 1994; Wyllie et al., 1998). It was suggested that hippocampal

GABAergic basket cells, which contain $\epsilon 4$ mRNA, do not have the $\epsilon 4$ type synaptic response of long kinetics and weak Mg^{2+} block (Catania et al., 1996). Moreover, some electrophysiological studies suggested that in the rat cerebellum $\epsilon 4$ is restricted to extrasynaptic sites and does not participate in synaptic transmission (Misra et al., 2000; Brickley et al., 2003).

Taken together, it is unlikely that $\zeta 1/\epsilon 4$ receptors are involved in synaptic transmission in hippocampal CA1 interneurons. The NMDA receptor composition is probably simplified to $\zeta 1$ and $\epsilon 2$ subunits as in pyramidal cell synapses in $\epsilon 1$ KO mice.

Asymmetrical NMDA receptor content in left and right pyramidal cell synapses

In wild type mouse, although the distinct amount of $\epsilon 2$ was found between left and right Sch-CA1 pyramidal cell synapses, the amplitude of NMDA EPSCs relative to that of non-NMDA EPSCs was the same in these synapses, indicating the same amount of NMDA receptor content between left and right Sch-CA1 pyramidal cell synapses (Fig. 8; Kawakami et al., 2003). However, in $\epsilon 1$ KO mice, since the NMDA subunit composition was simplified to $\zeta 1$ and $\epsilon 2$ in pyramidal cells (Sakimura et al., 1995), the amount of $\epsilon 2$ was directly reflected in the content of functional NMDA channels.

The CA1 pyramidal cells are innervated by the ipsilateral Schaffer collateral input and contralateral commissural (Com) fiber input. A complementary $\epsilon 2$ subunit contribution on the same cells depending on the side of input origin (ipsilateral or contralateral CA3 pyramidal cells) was suggested in wild type mice (Kawakami et al., 2003). Since the mean $\epsilon 2$ immunoparticle density was the same between the left and right hippocampus in naïve $\epsilon 1$ KO mice, on the basis of the asymmetrical $\epsilon 2$ distribution on Sch-CA1 synapses, a complementary $\epsilon 2$ distribution on Com-CA1

synapses with the dominant side opposite to that on Sch-CA1 synapses could be considered. This $\epsilon 2$ subunit organization enables the left and right Sch-CA1 and Com-CA1 synapses to progress the NMDA receptor-dependent synaptic plasticity differently in $\epsilon 1$ KO mice and also provides a model for studying the developmental input-selective regulation on NMDA receptor-dependent synaptic plasticity in wild-type mice, since in early postnatal rodents, the expression of $\epsilon 1$ subunit in hippocampus is still absent or very low compared with $\zeta 1$ and $\epsilon 2$ subunits (Monyer et al., 1994; Watanabe et al., 1992) and the NMDA subunit composition is similar to that in $\epsilon 1$ KO mice.

We also observed the asymmetrical allocation of $\epsilon 2$ between basal and apical Sch-CA1 pyramidal cell synapses at either left or right hippocampal CA1 area by postembedding method, being consistent with previous single cell recording that showed the asymmetrical $\epsilon 2$ content between apical and basal Sch-CA1 pyramidal cell synapses of wild type mice (Kawakami et al., 2003). Thus, the asymmetrical subunit allocation may be regulated by the polarity of the pyramidal neurons, e.g. the subunit allocation may be determined depending whether the receptors are located on the apical or basal dendrites.

$\zeta 1$ subunits allocation between left and right Sch-CA1 pyramidal cell synapses in $\epsilon 1$ KO mice

Functional NMDA receptors are heteromeric assemblies of $\zeta 1$ and ϵ subunits (Kutsuwada et al., 1992; Meguro et al., 1992). Analysis of the activation kinetic of native NMDA receptor channels revealed a kinetic model with at least two glutamate and two glycine binding sites (Benveniste and Mayer, 1991), indicating that NMDA

receptors were at least tetramers comprised of two each of $\zeta 1$ and ϵ subunits. Also, Sutcliffe et al. theoretically analyzed possible stoichiometries on NMDA receptor subunits and assumed tetrameric, pentameric, and hexameric assemblies (Sutcliffe et al., 1996). Some electrophysiological and biochemical studies also suggested that the NMDA receptor complexes were considered to consist of 2 or 3 $\zeta 1$ subunits and 2 or 3 ϵ subunits (Premkumar and Auerbach, 1997; Laube et al., 1998; Hawkins et al., 1999). Therefore, functional NMDA receptor complexes were assumed to consist of 2 or 3 $\zeta 1$ subunits and either 2 or 3 $\epsilon 2$ subunits in $\epsilon 1$ KO mice.

Western blot indicated the total amount of $\zeta 1$ subunit proteins was equal between left and right Sch-CA1 synapses in wild type mice (Kawakami et al., 2003). The functional NMDA channel number were the same between left and right Sch-CA1 synapses of the hippocampus in wild type mice. It was suggested that the knock out of a target ionotropic receptor subunit could alter other subunit expression at the synaptic sites (Forrest et al., 1994; Fukaya et al., 2003). Although in adult $\epsilon 1$ KO mice, the $\zeta 1$ expression at mRNA level had no appreciable difference compared with wild type mice (Sakimura, 1995), our electrophysiological results showed that the functional NMDA receptor abundance was asymmetrical between the left and right Sch-CA1 synapses of the hippocampus in $\epsilon 1$ KO mice. Since functional NMDA channels require the heteromeric assembly of $\zeta 1$ with $\epsilon 2$ subunit, not only the asymmetrical distribution of the $\epsilon 2$ subunit, but also that of the $\zeta 1$ may also occur in $\epsilon 1$ KO mice. For addressing this issue, I conducted postembedding immunogold method to detect immunoreactivity for $\zeta 1$ and found that the mean immunoparticle density for $\zeta 1$ on Sch-CA1 pyramidal cell synapses was not significantly different between the left and right stratum radiatum. This result suggests a possibility that there are more $\zeta 1$ subunits in NMDA receptor

heteromeric complexes or more ζ_1/ζ_1 homomeric complexes in the ϵ_2 non-dominant side than in the ϵ_2 dominant side of the hippocampus. In these cases, the amount of ζ_1 subunits could be same between the left and right hippocampus. Thus, the amount of ζ_1 seems to be kept constant and not directly reflected in the number of functional NMDA channels in synapses in ϵ_1 KO mice.

The physiological implications of left/right (L/R) asymmetry of ϵ_2 subunit

The physiological significance of the asymmetrical ϵ_2 allocation has not yet been understood. It has been suggested that ϵ_2 subunit plays an important role in LTP and learning and memory in the hippocampus (Tang et al., 2001; Clayton et al., 2002; Kramer et al., 2002). Furthermore, the left and right hippocampus has been suggested to contribute to the learning and memory differently (Bernasconi-Guastalla et al., 1994; Zaidel et al., 1998; Gagliardo et al., 2001). Elucidating precise allocation of the ϵ_2 subunit is thus of fundamental importance for further understanding of the function of the hippocampus and even the hippocampal left /right different contribution to learning and memory. The ϵ_1 KO mice with the enhanced difference in the NMDA receptor content would be a useful model for further investigation of the physiological significance of the asymmetry in hippocampal learning and memory.

Acknowledgement:

This project was supported by CREST from Japan Science and Technology Corporation. I thank Dr. Isao Ito and Dr. Ryosuke Kawakami for their electrophysiological study on this project. I thank Dr. Yasuyoshi Mishina, Dr. Kenji Sakimura and Dr. Hiroyuki Sugiyama for kindly providing the $\epsilon 1$ KO mice. I am grateful to Dr. Masahiro Fukaya, Dr. Masahiko Watanabe and Dr. Elek Molnar for kindly providing the antibodies.

References:

- Amaral DG, Witter MP, in *The Rat Nervous System*, G. Paxinos, Ed. (Academic Press, San Diego, CA, 1995), pp. 443–494.
- Baude A, Nusser Z, Roberts JD, Mulvihill E, McIlhinney RA, Somogyi P (1993) The metabotropic glutamate receptor (mGluR1 alpha) is concentrated at perisynaptic membrane of neuronal subpopulations as detected by immunogold reaction. *Neuron* 11:771-787.
- Bear MF, Malenka RC (1994) Synaptic plasticity: LTP and LTD. *Curr Opin Neurobiol* 4:389-399.
- Benveniste M, Mayer ML (1991) Kinetic analysis of antagonist action at N-methyl-D-aspartic acid receptors. Two binding sites each for glutamate and glycine. *Biophys J* 59:560-573.
- Bernasconi-Guastalla S, Wolfer DP, Lipp HP (1994) Hippocampal mossy fibers and swimming navigation in mice: correlations with size and left-right asymmetries. *Hippocampus* 4:53-63.
- Boulter J, Hollmann M, O'Shea-Greenfield A, Hartley M, Deneris E, Maron C, Heinemann S (1990) Molecular cloning and functional expression of glutamate receptor subunit genes. *Science* 249, 1033-1037
- Brickley SG, Misra C, Mok MH, Mishina M, Cull-Candy SG (2003) NR2B and NR2D subunits coassemble in cerebellar Golgi cells to form a distinct NMDA receptor subtype restricted to extrasynaptic sites. *J Neurosci* 23:4958-4966.
- Calverley RK, Jones DG (1987) Determination of the numerical density of perforated synapses in rat neocortex. *Cell Tissue Res* 248:399-407.

- Catania MV, Bellomo M, Giuffrida R, Stella AM, Albanese V (1998) AMPA receptor subunits are differentially expressed in parvalbumin- and calretinin-positive neurons of the rat hippocampus. *Eur J Neurosci* 10:3479-3490.
- Catania MV, Weishaupt J, Melcher T, Geiger JRP, Jonas P, Monyer H (1996) Glutamate receptor subunit composition in principal neurons and interneurons of the central nervous system. In: Conti F, Hicks TP (Eds), *Excitatory Amino Acids and the Cereb Cortex*. Cambridge, MA: MIT Press, pp 45-52
- Clayton DA, Mesches MH, Alvarez E, Bickford PC, Browning MD (2002) A hippocampal NR2B deficit can mimic age-related changes in long-term potentiation and spatial learning in the Fischer 344 rat. *J Neurosci* 22:3628-3637.
- Contractor A, Swanson GT, Sailer A, O'Gorman S, Heinemann SF (2000) Identification of the kainate receptor subunits underlying modulation of excitatory synaptic transmission in the CA3 region of the hippocampus. *J Neurosci* 20:8269-8278.
- Dingledine R, Borges K, Bowie D, Traynelis SF (1999) The glutamate receptor ion channels. *Pharmacol Rev* 51:7-61.
- Ferraguti F, Cobden P, Pollard M, Cope D, Shigemoto R, Watanabe M, Somogyi P (2004) Immunolocalization of metabotropic glutamate receptor 1alpha (mGluR1alpha) in distinct classes of interneuron in the CA1 region of the rat hippocampus. *Hippocampus* 14:193-215.
- Forrest D, Yuzaki M, Soares HD, Ng L, Luk DC, Sheng M, Stewart CL, Morgan JI, Connor JA, Curran T (1994) Targeted disruption of NMDA receptor 1 gene abolishes NMDA response and results in neonatal death. *Neuron* 13:325-338.
- Franklin K.B.J., Paxinos G (1997) *The mouse brain in stereotaxic Coordinates*

(Academic press).

- Freund TF, Buzsaki G (1996) Interneurons of the hippocampus. *Hippocampus* 6:347-470.
- Fritschy JM, Weinmann O, Wenzel A, Benke D (1998) Synapse-specific localization of NMDA and GABA(A) receptor subunits revealed by antigen-retrieval immunohistochemistry. *J Comp Neurol* 390:194-210.
- Fukaya M, Kato A, Lovett C, Tonegawa S, Watanabe M (2003) Retention of NMDA receptor NR2 subunits in the lumen of endoplasmic reticulum in targeted NR1 knockout mice. *Proc Natl Acad Sci U S A* 100:4855-4860.
- Gagliardo A, Ioale P, Odetti F, Bingman VP, Siegel JJ, Vallortigara G (2001) Hippocampus and homing in pigeons: left and right hemispheric differences in navigational map learning. *Eur J Neurosci* 13:1617-1624.
- Geiger JR, Melcher T, Koh DS, Sakmann B, Seeburg PH, Jonas P, Monyer H (1995) Relative abundance of subunit mRNAs determines gating and Ca²⁺ permeability of AMPA receptors in principal neurons and interneurons in rat CNS. *Neuron* 15:193-204.
- Gottmann K, Mehrle A, Gisselmann G, Hatt H (1997) Presynaptic control of subunit composition of NMDA receptors mediating synaptic plasticity. *J Neurosci* 17:2766-2774.
- Grosshans DR, Clayton DA, Coultrap SJ, Browning MD (2002) LTP leads to rapid surface expression of NMDA but not AMPA receptors in adult rat CA1. *Nat Neurosci* 5:27-33.
- Gulyas AI, Hajos N, Freund TF (1996) Interneurons containing calretinin are specialized to control other interneurons in the rat hippocampus. *J Neurosci*

16:3397-3411.

- Hawkins LM, Chazot PL, Stephenson FA (1999) Biochemical evidence for the co-association of three N-methyl-D-aspartate (NMDA) R2 subunits in recombinant NMDA receptors. *J Biol Chem* 274:27211-27218.
- Hashimoto K, Fukaya M, Qiao X, Sakimura K, Watanabe M, Kano M (1999) Impairment of AMPA receptor function in cerebellar granule cells of ataxic mutant mouse stargazer. *J Neurosci* 19:6027-6036.
- He Y, Janssen WG, Morrison JH (1998) Synaptic coexistence of AMPA and NMDA receptors in the rat hippocampus: a postembedding immunogold study. *J Neurosci Res* 54:444-449.
- Hollmann M, Heinemann S (1994) Cloned glutamate receptors. *Annu Rev Neurosci* 17:31-108.
- Ishizuka N, Weber J, Amaral DG (1990) Organization of intrahippocampal projections originating from CA3 pyramidal cells in the rat. *J Comp Neurol* 295:580-623.
- Ito I, Futai K, Katagiri H, Watanabe M, Sakimura K, Mishina M, Sugiyama H (1997) Synapse-selective impairment of NMDA receptor functions in mice lacking NMDA receptor epsilon 1 or epsilon 2 subunit. *J Physiol* 500 (Pt 2): 401-408.
- Ito I, Kawakami R, Sakimura K, Mishina M, Sugiyama H (2000) Input-specific targeting of NMDA receptor subtypes at mouse hippocampal CA3 pyramidal neuron synapses. *Neuropharmacology* 39:943-951.
- Kawakami R, Shinohara Y, Kato Y, Sugiyama H, Shigemoto R, Ito I (2003) Asymmetrical allocation of NMDA receptor epsilon2 subunits in hippocampal circuitry. *Science* 300:990-994.
- Kilbride J, Huang LQ, Rowan MJ, Anwyl R (1998) Presynaptic inhibitory action of the

- group II metabotropic glutamate receptor agonists, LY354740 and DCG-IV. *Eur J Pharmacol* 356:149-157.
- Kiyama Y, Manabe T, Sakimura K, Kawakami F, Mori H, Mishina M (1998) Increased thresholds for long-term potentiation and contextual learning in mice lacking the NMDA-type glutamate receptor epsilon1 subunit. *J Neurosci* 18:6704-6712.
- Klausberger T, Marton LF, Baude A, Roberts JD, Magill PJ, Somogyi P (2004) Spike timing of dendrite-targeting bistratified cells during hippocampal network oscillations in vivo. *Nat Neurosci* 7:41-47.
- Klausberger T, Magill PJ, Marton LF, Roberts JD, Cobden PM, Buzsaki G, Somogyi P (2003) Brain-state- and cell-type-specific firing of hippocampal interneurons in vivo. *Nature* 421:844-848.
- Kramer KL, Barnette JE, Yost HJ (2002) PKC γ regulates syndecan-2 inside-out signaling during xenopus left-right development. *Cell* 111:981-990.
- Kutsuwada T, Kashiwabuchi N, Mori H, Sakimura K, Kushiya E, Araki K, Meguro H, Masaki H, Kumanishi T, Arakawa M, et al. (1992) Molecular diversity of the NMDA receptor channel. *Nature* 358:36-41.
- Laube B, Kuhse J, Betz H (1998) Evidence for a tetrameric structure of recombinant NMDA receptors. *J Neurosci* 18:2954-2961.
- Liu SH, Wang J, Zhu DY, Fu YP, Lukowiak K, and Lu YM (2003) Generation of functional inhibitory neurons in the adult rat hippocampus. *J Neurosci* 23:732-736
- Losonczy A, Zhang L, Shigemoto R, Somogyi P, Nusser Z (2002) Cell type dependence and variability in the short-term plasticity of EPSCs in identified mouse hippocampal interneurons. *J Physiol* 542:193-210.

- Matsubara A, Laake JH, Davanger S, Usami S, Ottersen OP (1996) Organization of AMPA receptor subunits at a glutamate synapse: a quantitative immunogold analysis of hair cell synapses in the rat organ of Corti. *J Neurosci* 16:4457-4467.
- Matyas F, Freund TF, Gulyas AI (2004) Convergence of excitatory and inhibitory inputs onto CCK-containing basket cells in the CA1 area of the rat hippocampus. *Eur J Neurosci* 19:1243-1256.
- Meguro H, Mori H, Araki K, Kushiya E, Kutsuwada T, Yamazaki M, Kumanishi T, Arakawa M, Sakimura K, Mishina M (1992) Functional characterization of a heteromeric NMDA receptor channel expressed from cloned cDNAs. *Nature* 357:70-74.
- M.E. Rubio and R.J. Wenthold (1997) Glutamate receptors are selectively targeted to postsynaptic sites in neurons. *Neuron* 18: 939–950.
- Miettinen R, Gulyas AI, Baimbridge KG, Jacobowitz DM, Freund TF (1992) Calretinin is present in non-pyramidal cells of the rat hippocampus--II. Co-existence with other calcium binding proteins and GABA. *Neuroscience* 48:29-43.
- Misra C, Brickley SG, Farrant M, Cull-Candy SG (2000) Identification of subunits contributing to synaptic and extrasynaptic NMDA receptors in Golgi cells of the rat cerebellum. *J Physiol* 524 Pt 1:147-162.
- Monyer H, Burnashev N, Laurie DJ, Sakmann B, Seeburg PH (1994) Developmental and regional expression in the rat brain and functional properties of four NMDA receptors. *Neuron* 12:529-540.
- Nakanishi S (1992) Molecular diversity of glutamate receptors and implications for brain function. *Science* 258:597-603.
- Nakanishi S, Masu M (1994) Molecular diversity and functions of glutamate receptors.

- Ann Rev Biophys Biomol Struct 23:319-348.
- Nicoll RA, Malenka RC (1999) Expression mechanisms underlying NMDA receptor-dependent long-term potentiation. *Ann N Y Acad Sci* 868:515-525.
- Nitsch C, Goping G, Klatzo I (1989a) Preservation of GABAergic perikarya and boutons after transient ischemia in the gerbil hippocampal CA1 field. *Brain Res* 495:243-252
- Nitsch C, Scotti A, Sommacal A, Kalt G (1989b) GABAergic hippocampal neurons resistant to ischemia-induced neuronal death contain the Ca²⁺(+)-binding protein parvalbumin. *Neurosci Lett* 105:263-268.
- Nusser Z, Sieghart W, Somogyi P (1998a) Segregation of different GABA_A receptors to synaptic and extrasynaptic membranes of cerebellar granule cells. *J Neurosci* 18:1693-1703.
- Nusser Z, Sieghart W, Benke D, Fritschy JM, Somogyi P (1996) Differential synaptic localization of two major gamma-aminobutyric acid type A receptor alpha subunits on hippocampal pyramidal cells. *Proc Natl Acad Sci U S A* 93:11939-11944.
- Nusser Z, Lujan R, Laube G, Roberts JD, Molnar E, Somogyi P (1998b) Cell type and pathway dependence of synaptic AMPA receptor number and variability in the hippocampus. *Neuron* 21:545-559.
- Nyiri G, Stephenson FA, Freund TF, Somogyi P (2003) Large variability in synaptic N-methyl-D-aspartate receptor density on interneurons and a comparison with pyramidal-cell spines in the rat hippocampus. *Neuroscience* 119:347-363.
- Oliva AA, Jr., Jiang M, Lam T, Smith KL, Swann JW (2000) Novel hippocampal interneuronal subtypes identified using transgenic mice that express green

- fluorescent protein in GABAergic interneurons. *J Neurosci* 20:3354-3368.
- Petralia RS, Wang YX, Niedzielski AS, Wenthold RJ (1996) The metabotropic glutamate receptors, mGluR2 and mGluR3, show unique postsynaptic, presynaptic and glial localizations. *Neuroscience* 71:949-976.
- Pickard L, Noel J, Henley JM, Collingridge GL, Molnar E (2000) Developmental changes in synaptic AMPA and NMDA receptor distribution and AMPA receptor subunit composition in living hippocampal neurons. *J Neurosci* 20:7922-7931.
- Premkumar LS, Auerbach A (1997) Stoichiometry of recombinant N-methyl-D-aspartate receptor channels inferred from single-channel current patterns. *J Gen Physiol* 110:485-502.
- Racca C, Stephenson FA, Streit P, Roberts JD, Somogyi P (2000) NMDA receptor content of synapses in stratum radiatum of the hippocampal CA1 area. *J Neurosci* 20:2512-2522.
- Sakimura K, Kutsuwada T, Ito I, Manabe T, Takayama C, Kushiya E, Yagi T, Aizawa S, Inoue Y, Sugiyama H, et al. (1995) Reduced hippocampal LTP and spatial learning in mice lacking NMDA receptor epsilon 1 subunit. *Nature* 373:151-155.
- Seeburg PH (1993) The TINS/TiPS Lecture. The molecular biology of mammalian glutamate receptor channels. *Trends Neurosci* 16:359-365.
- Shigemoto R, Kulik A, Roberts JD, Ohishi H, Nusser Z, Kaneko T, Somogyi P (1996) Target-cell-specific concentration of a metabotropic glutamate receptor in the presynaptic active zone. *Nature* 381:523-525.
- Shigemoto R, Kinoshita A, Wada E, Nomura S, Ohishi H, Takada M, Flor PJ, Neki A, Abe T, Nakanishi S, Mizuno N (1997) Differential presynaptic localization of metabotropic glutamate receptor subtypes in the rat hippocampus. *J Neurosci*

17:7503-7522.

- Sloviter RS (1989) Calcium-binding protein (calbindin-D28k) and parvalbumin immunocytochemistry: localization in the rat hippocampus with specific reference to the selective vulnerability of hippocampal neurons to seizure activity. *J Comp Neurol* 280:183-196.
- Sprengel R, Suchanek B, Amico C, Brusa R, Burnashev N, Rozov A, Hvalby O, Jensen V, Paulsen O, Andersen P, Kim JJ, Thompson RF, Sun W, Webster LC, Grant SG, Eilers J, Konnerth A, Li J, McNamara JO, Seeburg PH (1998) Importance of the intracellular domain of NR2 subunits for NMDA receptor function in vivo. *Cell* 92:279-289.
- Standaert DG, Friberg IK, Landwehrmeyer GB, Young AB, Penney JB, Jr. (1999) Expression of NMDA glutamate receptor subunit mRNAs in neurochemically identified projection and interneurons in the striatum of the rat. *Brain Res Mol Brain Res* 64:11-23.
- Steward O, and Vinstan SL. (1983) The Process of Reinnervation in the Dentate Gyrus of the Adult Rat: A Quantitative Electron Microscopic Analysis of Terminal Proliferation and Reactive Synaptogenesis. *J Comp Neurol* 214:370-386.
- Sutcliffe MJ, Wo ZG, Oswald RE (1996) Three-dimensional models of non-NMDA glutamate receptors. *Biophys J* 70:1575-1589.
- Takumi Y, Ramirez-Leon V, Laake P, Rinvik E, Ottersen OP (1999) Different modes of expression of AMPA and NMDA receptors in hippocampal synapses. *Nat Neurosci* 2:618-624.
- Tang YP, Wang H, Feng R, Kyin M, Tsien JZ (2001) Differential effects of enrichment

- on learning and memory function in NR2B transgenic mice.
Neuropharmacology 41:779-790.
- Watanabe M, Inoue Y, Sakimura K, Mishina M (1992) Developmental changes in distribution of NMDA receptor channel subunit mRNAs. *Neuroreport* 3:1138-1140.
- Watanabe M, Inoue Y, Sakimura K, Mishina M (1993) Distinct distributions of five N-methyl-D-aspartate receptor channel subunit mRNAs in the forebrain. *J Comp Neurol* 338:377-390.
- Watanabe M, Fukaya M, Sakimura K, Manabe T, Mishina M, Inoue Y (1998) Selective scarcity of NMDA receptor channel subunits in the stratum lucidum (mossy fibre-recipient layer) of the mouse hippocampal CA3 subfield. *Eur J Neurosci* 10:478-487.
- Wyllie DJ, Behe P, Colquhoun D (1998) Single-channel activations and concentration jumps: comparison of recombinant NR1a/NR2A and NR1a/NR2D NMDA receptors. *J Physiol* 510 (Pt 1):1-18.
- Yamada K, Fukaya M, Shimizu H, Sakimura K, Watanabe M (2001) NMDA receptor subunits GluRepsilon1, GluRepsilon3 and GluRzeta1 are enriched at the mossy fibre-granule cell synapse in the adult mouse cerebellum. *Eur J Neurosci* 13:2025-2036.
- Zaidel DW, Esiri MM, Beardsworth ED (1998) Observations on the relationship between verbal explicit and implicit memory and density of neurons in the hippocampus. *Neuropsychologia* 36:1049-1062.

Figure and table legends:

Fig. 1 Axospinous asymmetrical synapse density reduction after VHCT operation in stratum radiatum of the CA1 region in $\epsilon 1$ KO mice

(A). Examples of normal spine synapses from the middle part of stratum radiatum of the CA1 area in naïve $\epsilon 1$ KO mice (arrows). Arrows indicated normal axospinous asymmetrical synapses. Scale bar: 200nm

(B). A representative area from the middle part of stratum radiatum of the CA1 area in VHCT operated $\epsilon 1$ KO mice. A commissure fiber terminal (arrow) displayed the typical electron-dense type of degeneration. Scale bar: 200nm

(C). No significant difference in synapse density was detected between left and right stratum radiatum of the CA1 area in naïve $\epsilon 1$ KO mice ($1.61 \pm 0.09/\mu\text{m}^3$ and $1.63 \pm 0.05/\mu\text{m}^3$ respectively, $n=3$, t -test $P>0.05$). The mean axospinous asymmetrical synapse densities decreased to $1.01 \pm 0.01 /\mu\text{m}^3$ and $0.99 \pm 0.05 /\mu\text{m}^3$ respectively in left and right stratum radiatum of the CA1 area 5 days after VHCT operation (t -test ** $P<0.01$, compared with respective naïve group) and there were no significant difference between left and right stratum radiatum of the CA1 area. ($n=3$ animals, t -test $P>0.05$).

Fig. 2 Immunogold labeling for $\epsilon 2$, $\zeta 1$ and GluR2/3 on pyramidal cell synapses in hippocampal CA1 area

(A) Immunogold labeling for $\epsilon 2$ in stratum radiatum of hippocampal CA1 area in $\epsilon 1$ KO naïve mouse (mouse 5) as demonstrated by 5nm gold particles. Immunogold particles were concentrated at asymmetrical postsynaptic membrane specializations,

postsynaptic densities or the synaptic cleft of the pyramidal cells in stratum radiatum of CA1 area (arrows). Scale bar: 200nm

(B) Immunogold labeling for $\epsilon 2$ in stratum radiatum of hippocampal CA1 area in $\epsilon 1$ KO VHCT operated mouse (mouse 4) as demonstrated by 5nm gold particles. Immunogold particles were mainly concentrated at the type 1 postsynaptic membrane specializations, postsynaptic densities or the synaptic cleft of the pyramidal cells in CA1 area (arrows). Scale bar: 200nm

(C) Immunogold labeling for GluR2/3 in stratum radiatum of hippocampal CA1 area in $\epsilon 1$ KO VHCT operated mice as demonstrated by 5nm gold particles. Immunogold particles were mainly concentrated at the asymmetrical postsynaptic membrane specializations, postsynaptic densities or the synaptic cleft of the pyramidal cells in stratum radiatum of CA1 area (arrows), also several immunogold particles were located at the extrasynaptic membrane (open arrow). Scale bar: 200nm

(D) Immunogold labeling for $\zeta 1$ in stratum radiatum of hippocampal CA1 area in $\epsilon 1$ KO VHCT operated mice as demonstrated by 5nm gold particles. Immunogold particles were concentrated mainly at the asymmetrical postsynaptic membrane specializations, postsynaptic densities or occasionally at the synaptic cleft of the pyramidal cells in stratum radiatum of CA1 area (arrows). Scale bar: 200nm

Fig. 3 Asymmetrical $\epsilon 2$ subunit distribution between left and right and between basal and apical Sch-CA1 pyramidal cell synapses

(A) The $\epsilon 2$ labeling density showed a significant difference in distribution (mouse 1, n as in Table 2, Kolmogorov-Smirnov test, $P < 0.05$) between the left and right stratum oriens. The similar results were obtained from other 2 mice (mouse2, 4).

(B) The $\epsilon 2$ labeling density showed a significant difference in distribution (mouse 1, n as in Table 2, Kolmogorov-Smirnov test, $P < 0.05$) between the left and right stratum radiatum. The similar results were obtained from other 3 mice (mouse 2, 3, 4).

(C) The cumulative probability curve in right stratum oriens was homogeneously shifted to right compared with that in the left stratum oriens (mouse 1, n as in Table 2, Kolmogorov-Smirnov test, $P < 0.05$). The similar results were obtained from other 2 mice (mouse 2, 4).

(D) The cumulative probability curve in left stratum radiatum was homogeneously shifted to right compared with that in the left stratum radiatum (mouse 1, n as in Table 2, Kolmogorov-Smirnov test, $P < 0.05$). The similar results were obtained from other 3 mice (mouse 2, 3, 4).

(E) The cumulative probability curve in left apical dendrites was homogeneously shifted to right compared with that in the left basal dendrites (mouse 1, n as in Table 2, Kolmogorov-Smirnov test, $P < 0.05$). The similar results were obtained from other 2 mice (mouse 2, 4).

(F) The cumulative probability curve in right basal dendrites was homogeneously shifted to right compared with that in the right apical dendrites (mouse 1, n as in Table 2, Kolmogorov-Smirnov test, $P < 0.05$). The similar results were obtained from other 2 mice (mouse 2, 4).

Fig. 4 Co-localization of GluR4 with PV and mGluR1 α in hippocampal CA1 area

(A1) Cell bodies of the GluR4 immunopositive interneurons were mainly localized in the stratum pyramidale and adjoining stratum oriens (arrows). The GluR4 staining was also localized on the radially oriented dendrites of immunoreactive neurons in both

stratum oriens and stratum radiatum. Note the pyramidal cells were immunonegative for GluR4.

(A2) The soma of the interneurons in and near the pyramidal cell layer was strongly immunopositive for parvalbumin (arrows).

(A3) The overlap of the soma of the GluR4 immunopositive neurons and PV immunopositive interneurons was evident. (arrows).

(B1) The interneuron soma (arrow) and the numerous dendrites (asterisk) in str. oriens or alveus were intensely GluR4-immunolabeled.

(B2) The soma (arrow) and dendrites (asterisk) of mGluR1 α immunopositive interneuron were found mainly in the alveus and adjoining str. oriens in the CA1 area.

(B3) The overlap of the soma of the GluR4 immunopositive interneurons and mGluR1 α immunopositive interneurons was evident. (arrows).

Fig. 5 The absent of immunoreactivity for GluR4 from Calbindin (CB) and Calretinin (CR) immunoreactive interneurons in hippocampal CA1 area

(A1, B1) Cell bodies of the GluR4-immunopositive interneurons were mainly presented in the stratum pyramidale (Fig. 5A1, B1).

(A2) Strongly CB-immunopositive neurons present in distal one-third of the stratum radiatum, and some superficially located pyramidal cells also weakly expressed CB. Note the terminals containing CB appeared to delineate the soma.

(A3) No overlap was found between GluR4- and CB-immunopositive interneurons.
Scale bar: 50 μ m

(B2) The CR- immunopositive interneurons were frequently found in the interneurons in stratum pyramidale. Note the terminals containing CR appeared to delineate the

soma.

(B3) No overlap was found between GluR4- and CR- immunopositive interneurons.

Scale bar: 50 μ m

Fig. 6 Immunogold labeling for ϵ 2 on Sch-CA1 interneuron synapses in hippocampal CA1 area

(A, B) 5nm immunogold particles for ϵ 2 were found in type 1 synapses on dendritic shafts. Immunoparticles mainly concentrated at the postsynaptic membrane of asymmetric dendritic shaft, synaptic cleft or sometimes presynaptic membrane (filled arrows). Scale bar: 200nm

(C) Immunogold labeling for ϵ 2 (5nm) in GluR4 (10nm) immunopositive type 1 synapses on dendritic shafts. 5nm immunogold particles for ϵ 2 (filled arrows) were mainly concentrated at the postsynaptic membrane of asymmetric dendritic shaft, synaptic cleft or occasionally presynaptic membrane. Moderate 10 nm particle labelings for GluR4 (open arrows) were found in type 1 synapses on dendritic shafts. Scale bar: 200nm

Fig. 7 The summary of Left/Right ratio for ϵ 2, ζ 1 and GluR2/3 immunoparticle density on Sch-CA1 neuron synapses of stratum radiatum.

The mean Left/right ratio for ϵ 2 in Sch-CA1 pyramidal cell synapses was 1.63 ± 0.21 (n=4, Paired *t*-test $P < 0.05$). The mean Left/Right ratio for ϵ 2 in Sch-GluR4-positive interneuron synapses was 0.88 ± 0.04 (n=3, Paired *t*-test $P > 0.05$). The mean Left/Right ratio for ϵ 2 in Sch-GluR4-negative interneuron synapses was 1.14 ± 0.12 (n=3, Paired *t*-test $P > 0.05$). The mean Left/Right ratio for ζ 1 in Sch-CA1 pyramidal cell synapses

was 1.13 ± 0.18 ($n=4$, Paired t -test $P>0.05$). The mean Left/Right ratio for GluR2/3 in Sch-CA1 pyramidal cell synapses was 0.94 ± 0.06 ($n=4$, Paired t -test $P>0.05$). Pyra, pyramidal cells; Inter, interneurons.

Fig. 8 Left-Right asymmetry of NMDA response on Sch-CA1 synapses in $\epsilon 1$ subunit KO mice

(A) Schematic diagrams show the arrangement of electrodes for recording. To activate Schaffer collateral fibers to CA1 stratum oriens, a stimulating electrode was placed in the CA1 stratum oriens. Whole- cell patch recordings were made from CA1 pyramidal neurons. Sample superimposed traces showed representative EPSCs recorded in hippocampal slices prepared from WT mice and $\epsilon 1$ subunit KO mice. Upper traces showed NMDA EPSCs at +30mV in the presence of DNQX and bicuculline. Lower traces showed non-NMDA EPSCs at -90mV in the presence of bicuculline. Each trace was the average of five consecutive recordings. Relative amplitudes of NMDA EPSCs were expressed as percentages of control responses. Columns and error bars represented means and SEM respectively ($n=5$ each, *** $P<0.01$, absence of an asterisk indicates $P>0.05$).

(B) Schematic diagrams showed the arrangement of electrodes for recording. To activate Schaffer collateral fibers to CA1 stratum radiatum, a stimulating electrode was placed in the CA1 stratum radiatum. The others were the same as those described in (A) ($n=5$ each, ** $P<0.05$, *** $P<0.01$, absence of an asterisk indicates $P>0.05$). Bars were 50pA and 100ms.

Fig. 9 Asymmetry in LTP in the left and right Sch-CA1 stratum radiatum of $\epsilon 1$ KO VHCT mice

Upper schematic diagrams showed synaptic inputs on the apical dendrites of CA1 pyramidal neurons and arrangement of electrodes for extracellular recording. fEPSP were recorded by an extracellular electrode placed in the stratum radiatum of CA1 area and electrical stimuli were applied at Shaffer fibers of the same subfield. Middle panel showed the LTP amplitude induced in the left and right Sch-CA1 radiatum in wild type and $\epsilon 1$ knock out VHCT operated mice. Arrows indicated the time point at which a tetanic stimulation was given. Symbols and error bars represented means and SEM respectively (n=5-7). Lower traces showed representative fEPSP recorded before (1) and after (2) tetanic stimulation in the left and right Sch-CA1 radiatum of wild type and $\epsilon 1$ knock out VHCT operated mice respectively.

Table 1. Summary of the comparisons of the mean densities for $\epsilon 2$ on pyramidal cell synapses between left and right hippocampus in wild type mice. There was no significantly different mean density for $\epsilon 2$ between left and right hippocampus in all animals. Comparisons were made within the same sections to ensure identical incubation conditions in each animal group. Abbreviations: Mean density, number of particles/length of postsynaptic density (μm); Left, left hippocampus; Right, right hippocampus; SE, standard error; M-W test, Man-Whitney *U* test; VHCT, ventral hippocampal commissure transection.

Table 2. Summary of the comparisons of the mean densities for $\epsilon 2$, $\zeta 1$, and GluR2/3 on pyramidal cell synapses between left and right hippocampus in $\epsilon 1$ KO mice.

Comparisons were made within the same sections to ensure identical incubation conditions in each animal group. Abbreviations: Mean density, number of particles/length of postsynaptic density (μm); Left, left hippocampus; Right, right hippocampus; SE, standard error; M-W test, Man-Whitney *U* test; VHCT, ventral hippocampal commissure transection.

Table 3. Summary of the comparisons of the mean densities for $\epsilon 2$ in Sch-CA1 interneuron synapses between left and right hippocampus in $\epsilon 1$ KO mice. Comparisons were made within the same sections to ensure identical incubation conditions in each animal group. Abbreviations: Mean density, number of particles/length of postsynaptic density (μm); SE, standard error; M-W test, Man-Whitney *U* test; VHCT, ventral hippocampal commissure transection.

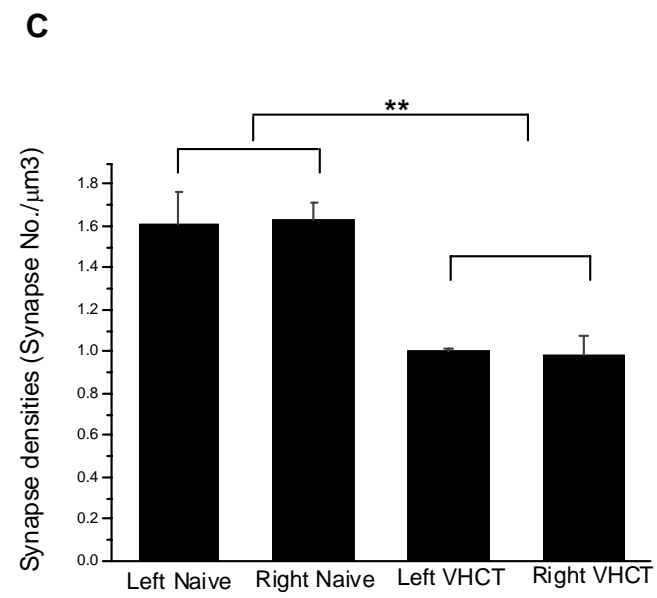
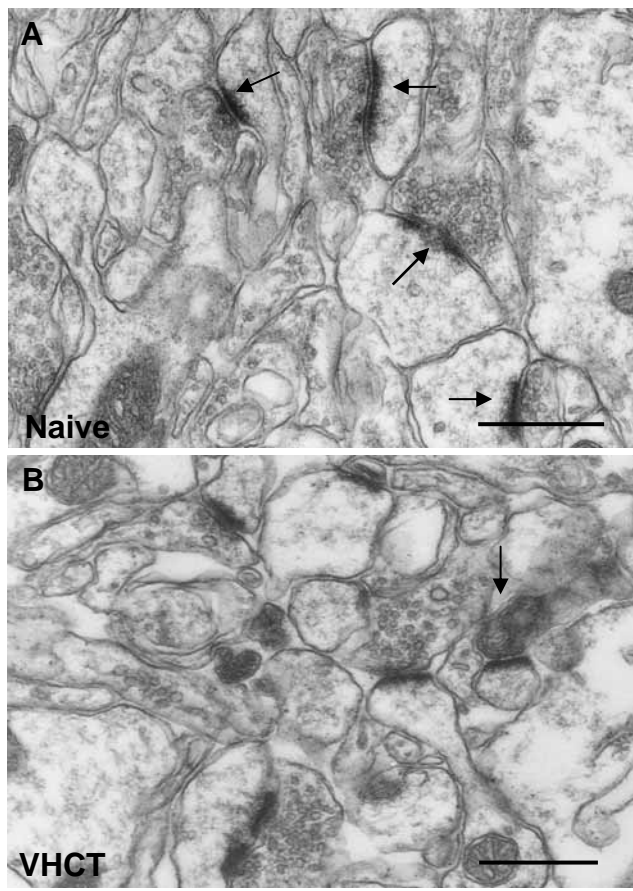


Fig. 1

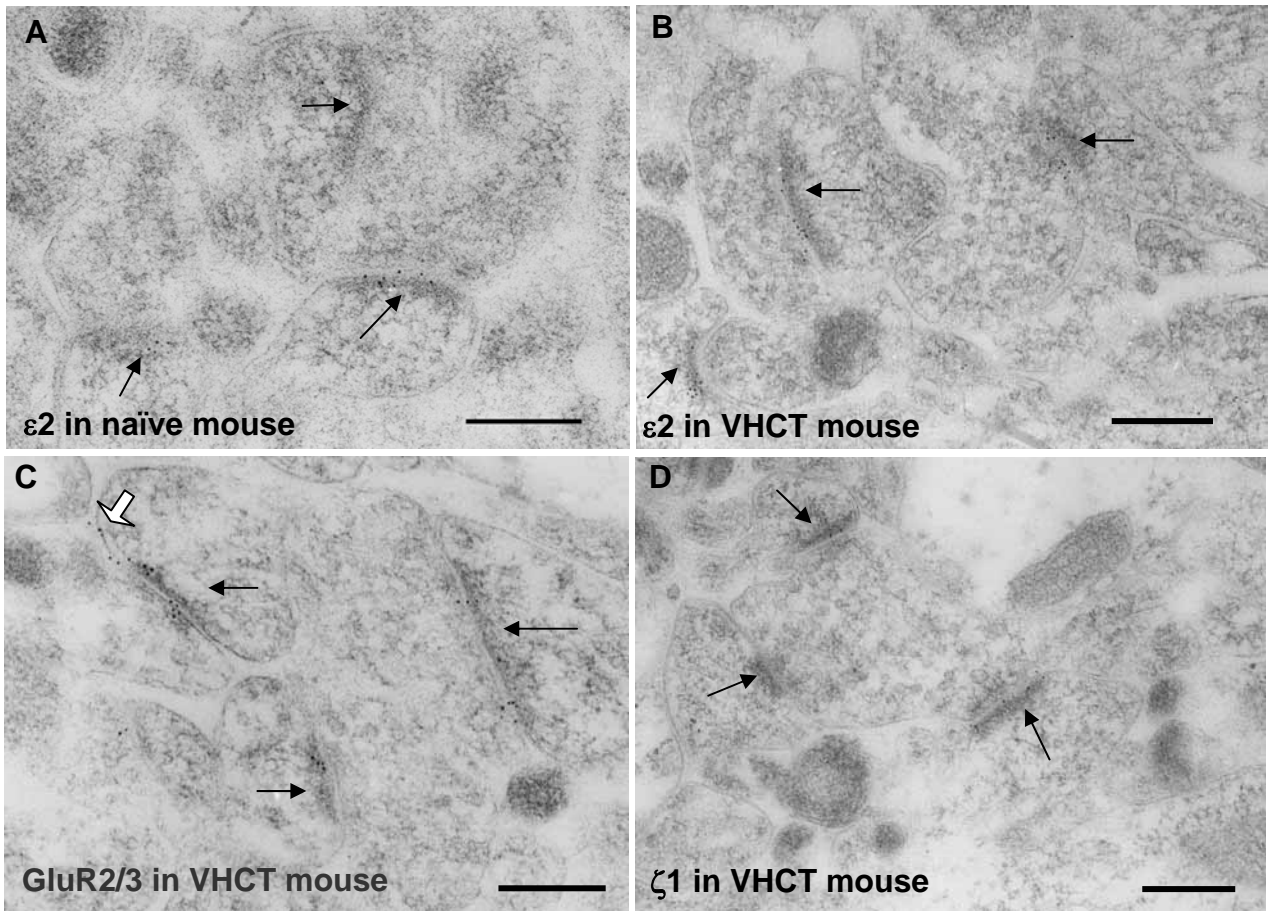


Fig. 2

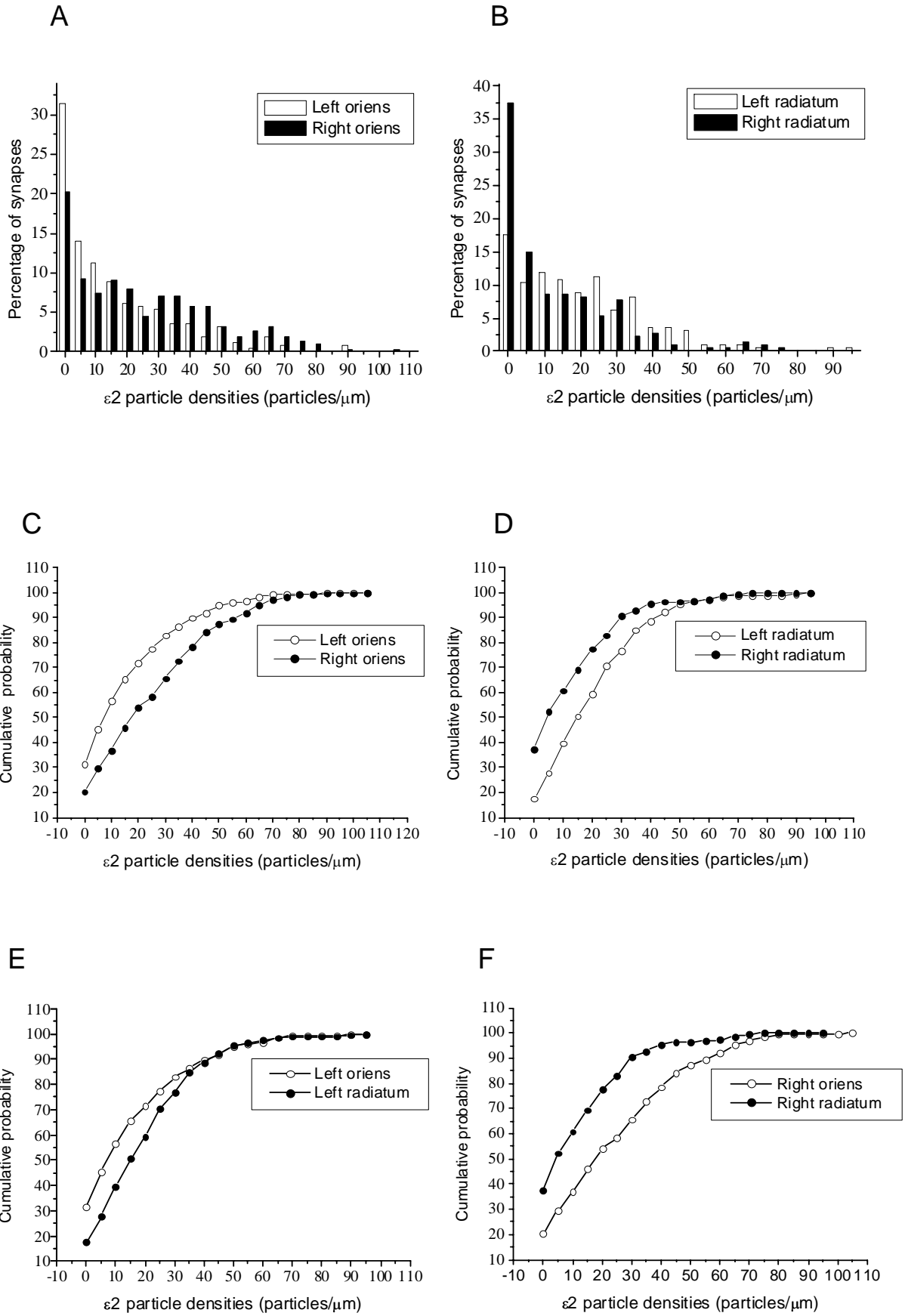


Fig. 3

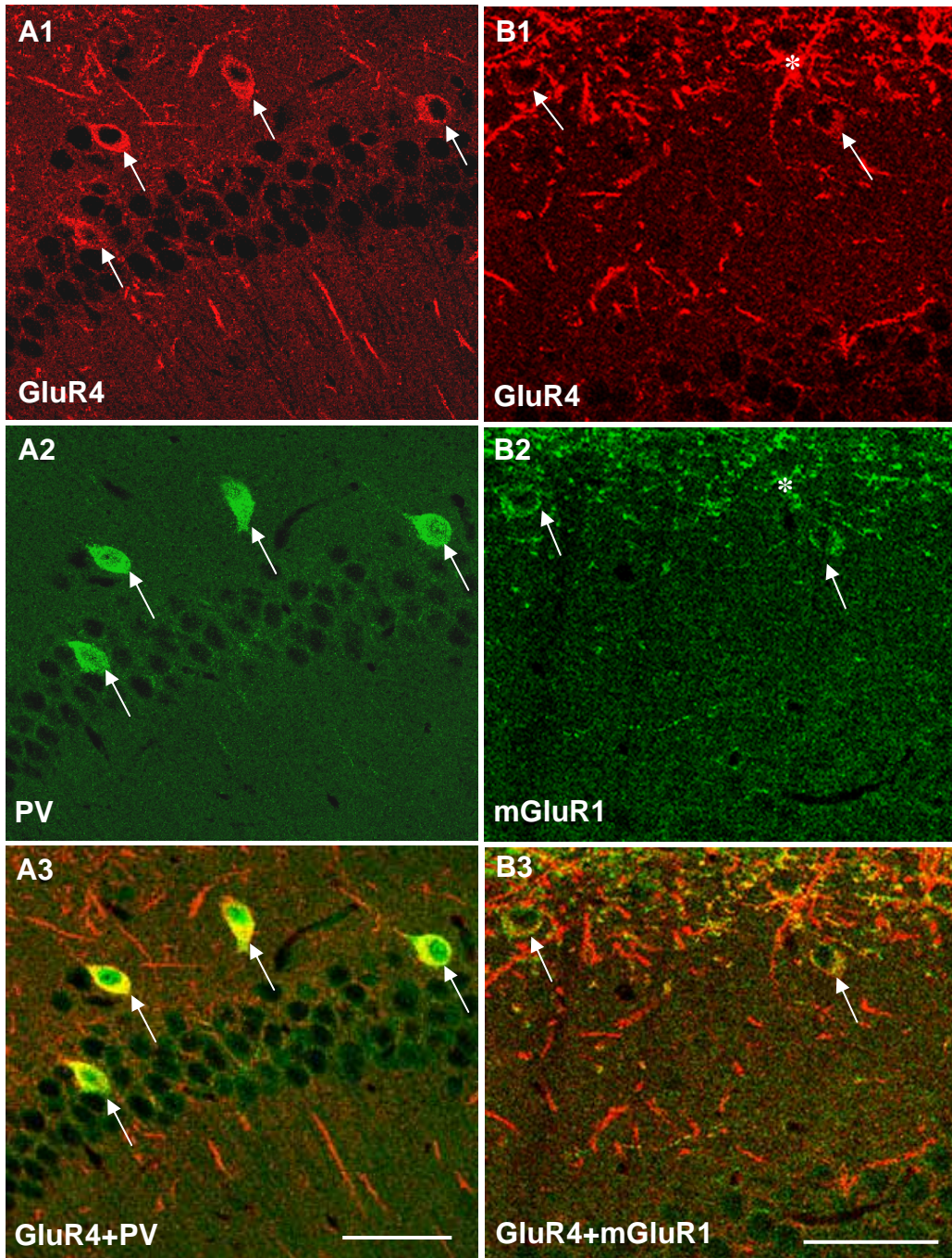


Fig. 4

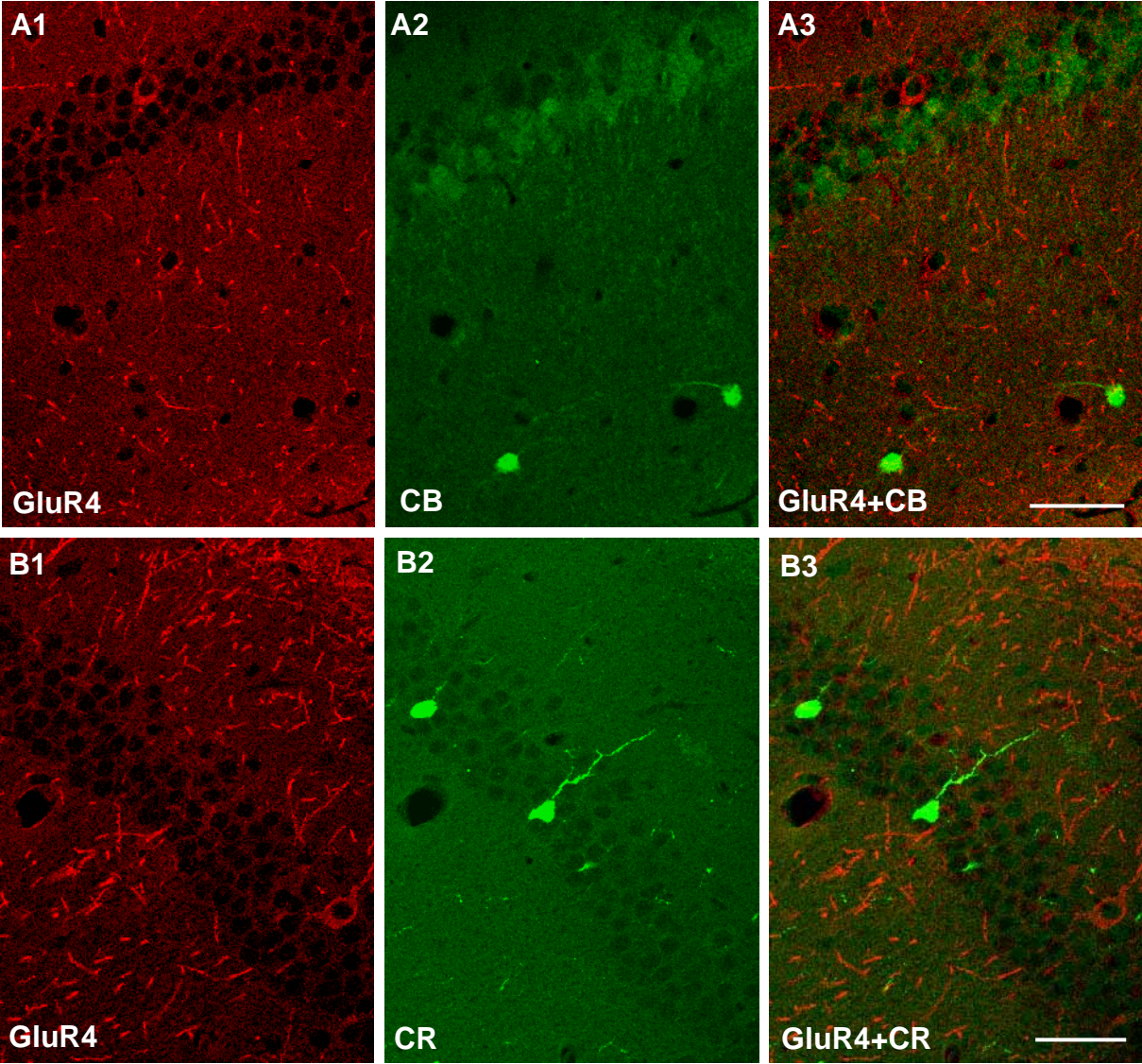


Fig. 5

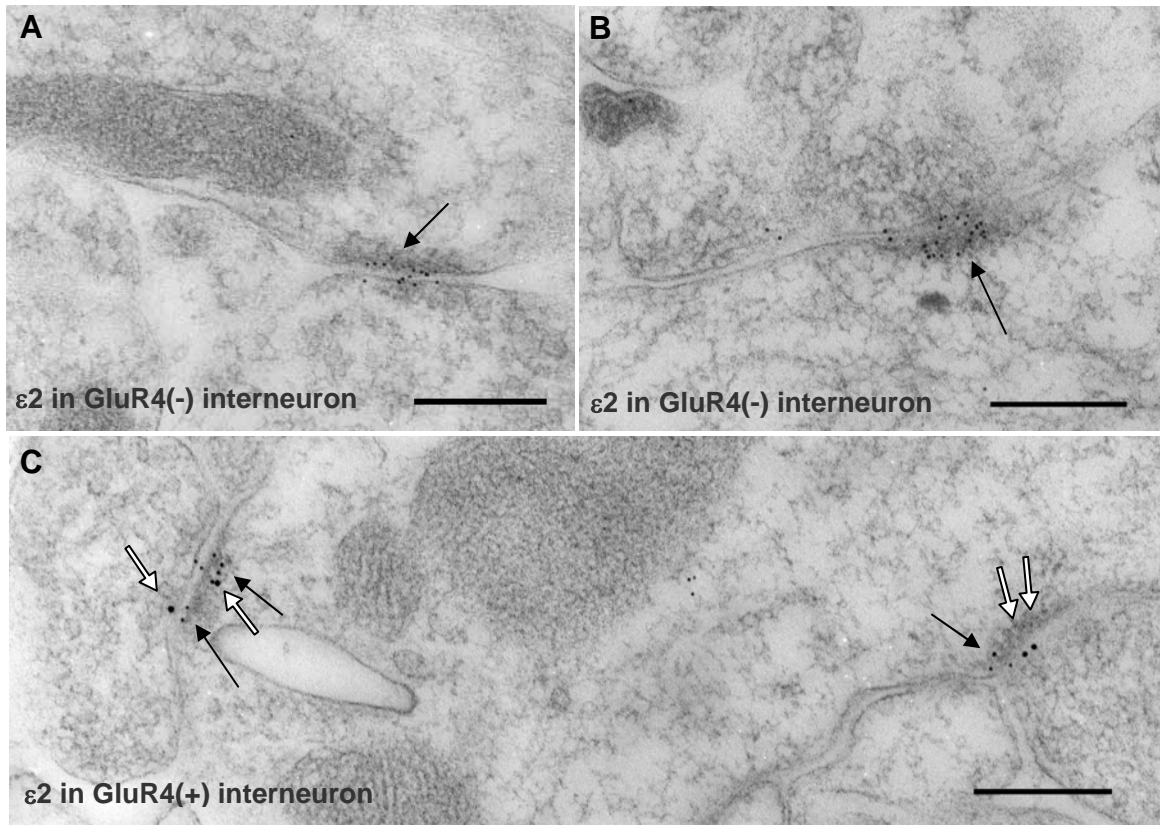


Fig. 6

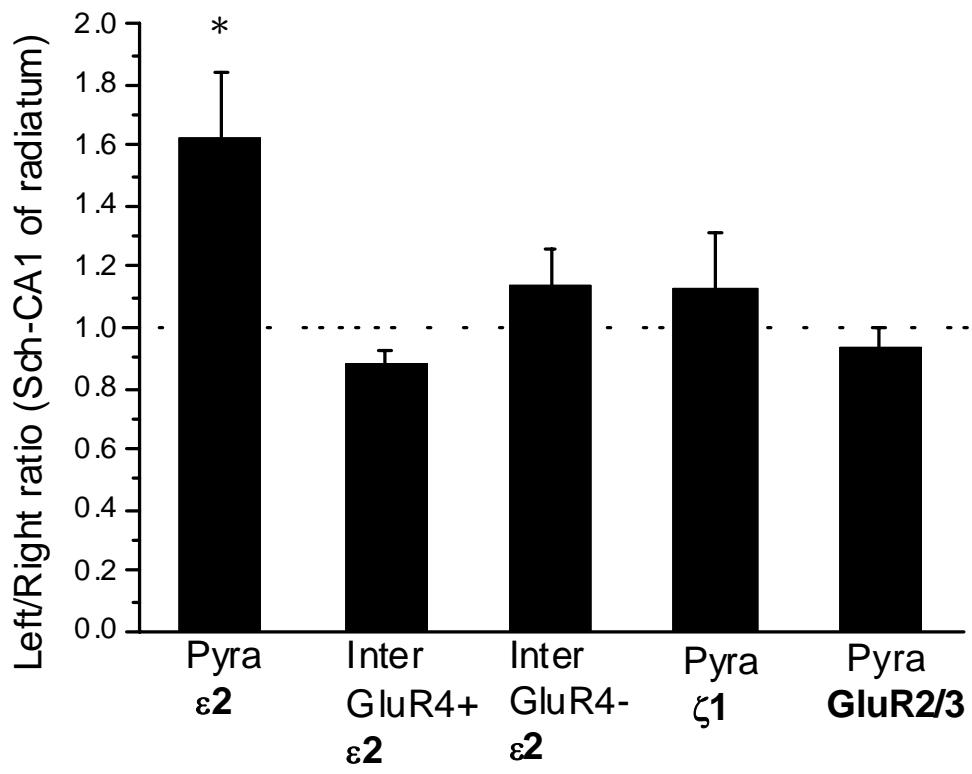


Fig. 7

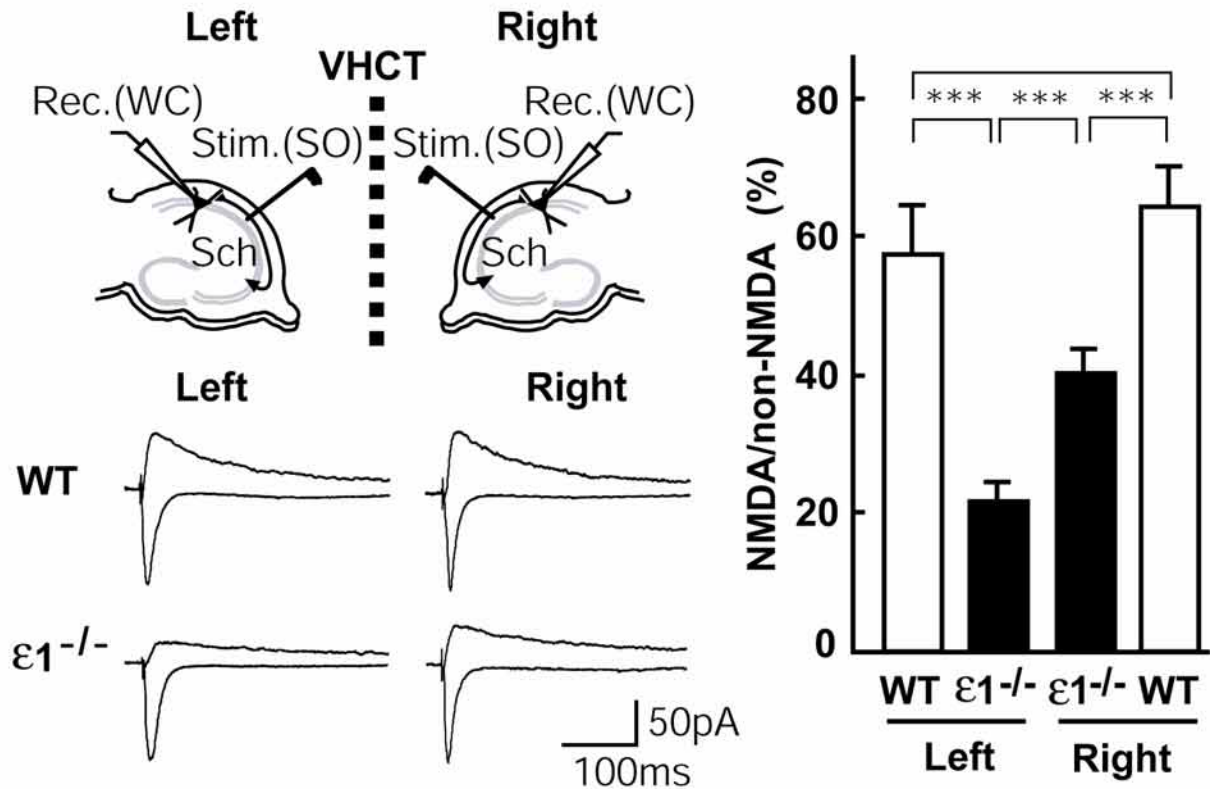
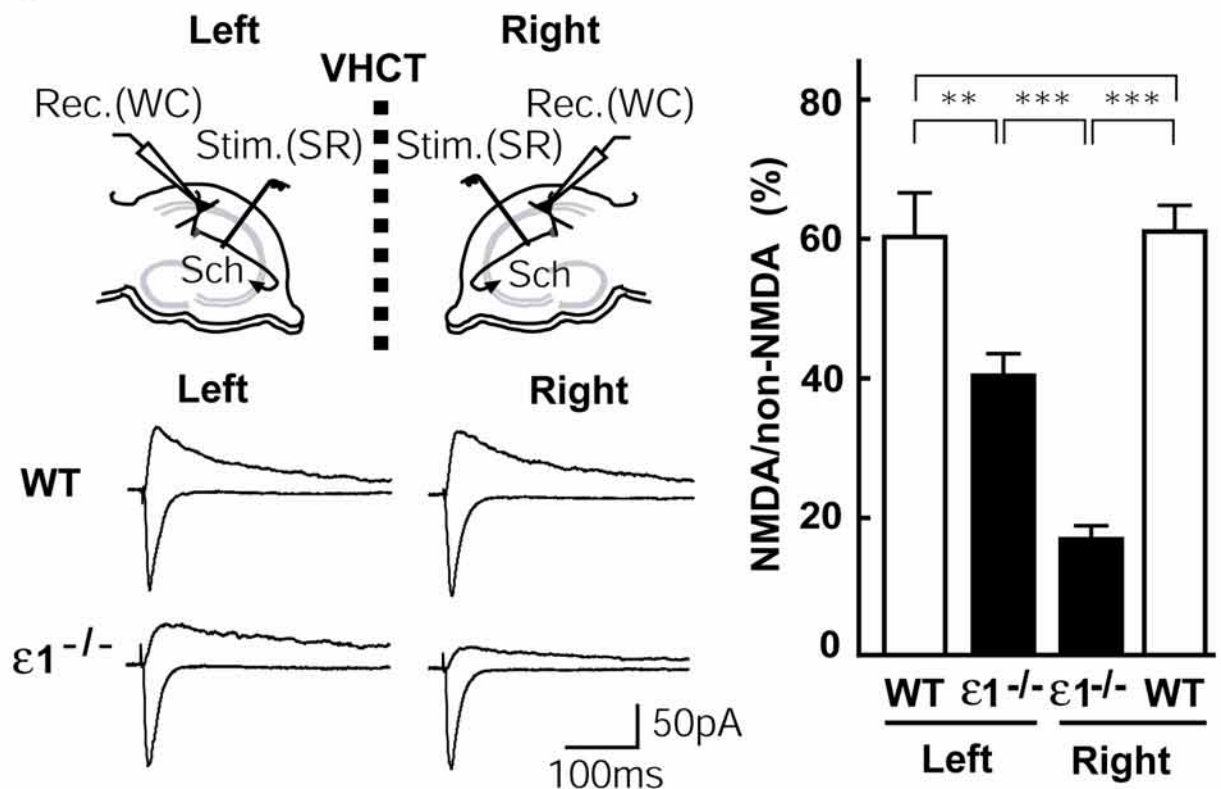
A**B**

Fig.8

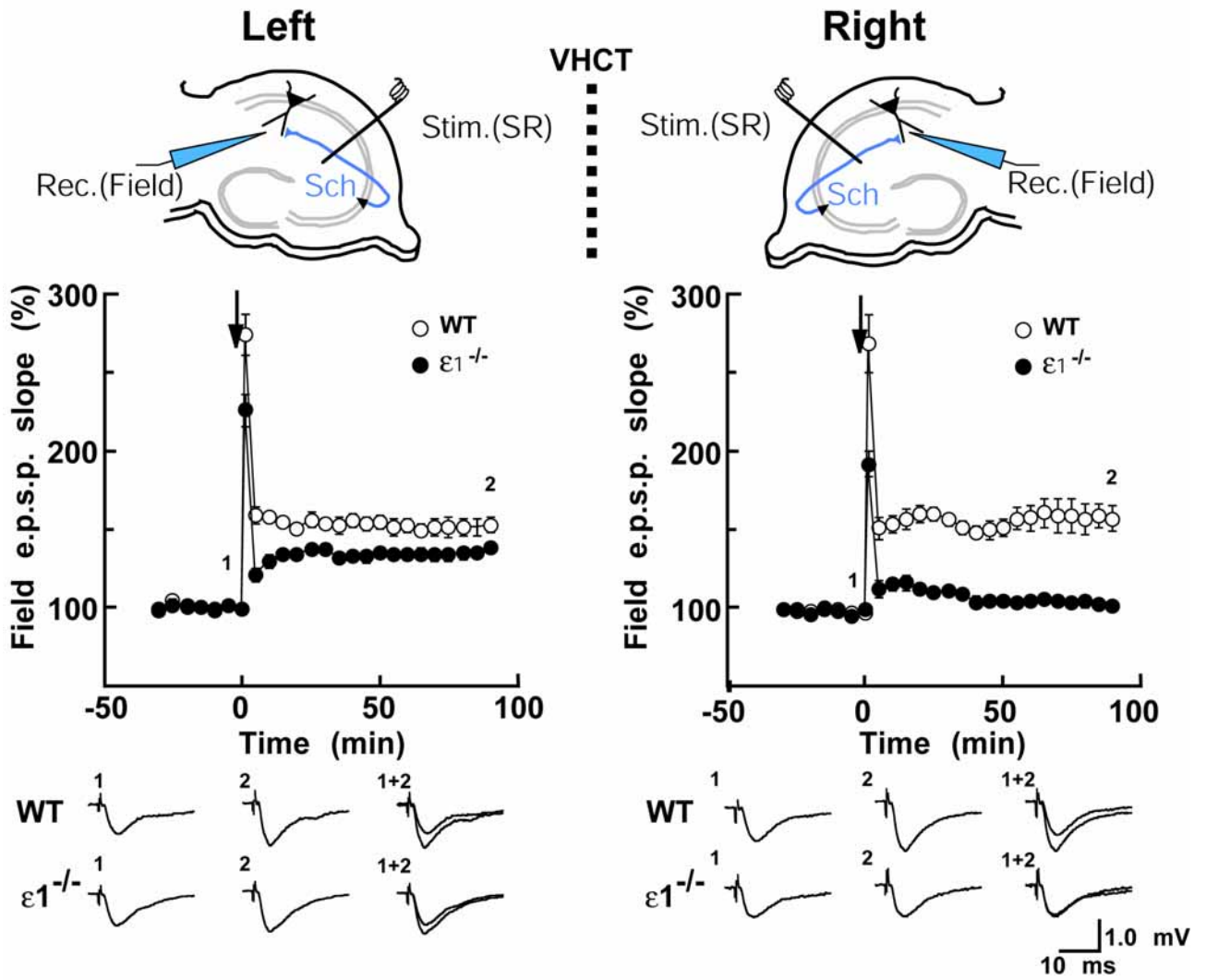


Fig. 9

Table 1 $\epsilon 2$ in pyramidal cells of wild type mice

Animal operation	Animal No.	stratum	Mean density (particle number/ μm) for $\epsilon 2 \pm \text{SE}$ (synapse number)		M-W test	Paired t -test
			Left	Right		
Naive	8	oriens	11.63 \pm 0.84 (206)	14.85 \pm 1.11(196)	P>0.05	
	8	radiatum	12.74 \pm 1.33 (166)	13.97 \pm 1.07 (195)	P>0.05	P>0.05
	11	radiatum	52.39 \pm 3.98 (51)	52.26 \pm 4.49 (39)	P>0.05	
	12	radiatum	32.20 \pm 2.81 (61)	29.02 \pm 3.54 (71)	P>0.05	
VHCT	9	oriens	11.72 \pm 1.14(127)	14.80 \pm 1.38 (106)	P>0.05	
	10	oriens	13.51 \pm 1.54 (103)	13.66 \pm 1.49 (74)	P>0.05	
	9	radiatum	10.51 \pm 1.14 (118)	13.08 \pm 1.31 (123)	P>0.05	P>0.05
	10	radiatum	11.91 \pm 1.18 (100)	11.22 \pm 1.19 (104)	P>0.05	
	13	radiatum	31.40 \pm 3.31 (57)	28.44 \pm 2.38 (65)	P>0.05	
	14	radiatum	25.75 \pm 2.35 (64)	29.94 \pm 2.74 (53)	P>0.05	

Table 2 NMDA subunits in pyramidal cells of $\epsilon 1$ KO mice

Animal operation	Animal No.	Subunits	Stratum	Mean density (particle number/ μm) \pm SE (synapse number)		M-W test	Paired <i>t</i> -test
				Left	Right		
Naïve	5	$\epsilon 2$	oriens	17.92 \pm 0.91(429)	15.10 \pm 0.83 (329)	P>0.05	P>0.05
	6			12.69 \pm 1.68 (80)	13.29 \pm 1.26 (120)	P>0.05	
	5	radiatum	20.24 \pm 1.35 (139)	21.43 \pm 1.52 (169)	P>0.05		
	6		15.76 \pm 1.66 (115)	13.36 \pm 1.49 (102)	P>0.05		
	7		10.95 \pm 1.06 (199)	12.39 \pm 1.10 (177)	P>0.05		
	5	$\zeta 1$	radiatum	18.25 \pm 1.30 (165)	17.03 \pm 1.25 (154)	P>0.05	
	6			8.83 \pm 0.89 (161)	11.11 \pm 1.09 (161)	P>0.05	
	5	GluR2/3	radiatum	26.26 \pm 2.31 (101)	25.45 \pm 2.10 (109)	P>0.05	
6	18.49 \pm 1.82 (77)			22.67 \pm 2.53 (78)	P>0.05		
VHCT	1	$\epsilon 2$	oriens	17.57 \pm 1.19 (311)	26.84 \pm 1.69 (259)	P<0.05	P<0.05
	2			20.74 \pm 1.49 (195)	29.89 \pm 1.64 (201)	P<0.05	
	4			21.80 \pm 1.59 (153)	33.31 \pm 1.69 (153)	P<0.05	
	1	radiatum	22.53 \pm 1.31 (222)	14.49 \pm 1.11(194)	P<0.05	P<0.05	
	2		31.55 \pm 2.05 (121)	20.01 \pm 1.54 (129)	P<0.05		
	3		15.90 \pm 0.83 (327)	7.21 \pm 0.63 (243)	P<0.05		
	4		27.58 \pm 1.61 (191)	23.33 \pm 1.69 (166)	P<0.05		
	1	$\zeta 1$	radiatum	20.33 \pm 1.76 (92)	21.00 \pm 1.72 (99)	P>0.05	P>0.05
	2			17.88 \pm 1.42 (152)	19.52 \pm 1.45 (130)	P>0.05	
	3			11.87 \pm 1.37 (99)	7.06 \pm 0.91 (114)	P<0.05	
	4			8.45 \pm 0.78 (177)	8.77 \pm 0.94 (167)	P>0.05	
	1	GluR2/3	radiatum	37.00 \pm 3.41 (67)	41.07 \pm 4.24 (65)	P>0.05	P>0.05
	2			23.77 \pm 2.79 (81)	29.71 \pm 2.92 (79)	P>0.05	
	3			24.25 \pm 2.19 (93)	22.08 \pm 2.21 (86)	P>0.05	
	4			24.14 \pm 2.01 (85)	24.66 \pm 2.21 (62)	P>0.05	

Table3 $\epsilon 2$ in interneurons of VHCT $\epsilon 1$ KO mice

Interneuron types	Animal No.	Mean density (particle number/ μm) for $\epsilon 2$ \pm SE (synapse number)		M-W test	Paired <i>t</i> test
		Left radiatum	Right radiatum		
GluR4 positive	1	11.87 \pm 3.53 (14)	13.13 \pm 2.40 (28)	P>0.05	P>0.05
	2	3.35 \pm 1.21 (11)	3.54 \pm 1.17 (21)	P>0.05	
	3	9.49 \pm 3.18 (21)	11.87 \pm 4.40 (10)	P>0.05	
GluR4 negative	1	36.84 \pm 4.46 (39)	31.60 \pm 4.45 (19)	P>0.05	P>0.05
	2	17.30 \pm 3.52 (14)	18.66 \pm 3.66 (19)	P>0.05	
	3	26.77 \pm 3.27 (19)	20.02 \pm 3.42 (28)	P>0.05	

